ISSN 1075-7015, Geology of Ore Deposits, 2016, Vol. 58, No. 5, pp. 383–403. © Pleiades Publishing, Ltd., 2016.
Original Russian Text © A.V. Kargin, A.A. Nosova, A.V. Postnikov, A.V. Chugaev, O.V. Postnikova, L.P. Popova, V.V. Poshibaev, L.V. Sazonova, A.Ya. Dokuchaev, M.D. Smirnova, 2016, published in Geologiya Rudnykh Mestorozhdenii, 2016, Vol. 58, No. 5, pp. 430–450.

Devonian Ultramafic Lamprophyre in the Irkineeva–Chadobets Trough in the Southwest of the Siberian Platform: Age, Composition, and Implications for Diamond Potential Prediction

A. V. Kargin[a, *], A. A. Nosova[a], A. V. Postnikov[b], A. V. Chugaev[a], O. V. Postnikova[b, **], L. P. Popova[b], V. V. Poshibaev[b], L. V. Sazonova[a], A. Ya. Dokuchaev[a], and M. D. Smirnova[a]

[a] *Institute of Geology of Ore Deposits, Petrography, Mineralogy and Geochemistry, Russian Academy of Sciences, Moscow, 119117 Russia*

[b] *Gubkin Russian State University of Oil and Gas (National Research University), Moscow, 110991 Russia*

**e-mail: kargin@igem.ru*

***e-mail: olgapostnikova@yandex.ru*

Received January 12, 2016

Abstract—The results of geochronological, mineralogical, petrographical, and geochemical study of the Ilbokich ultramafic lamprophyre are reported. The specific features in the mineral and chemical compositions of the studied ultramafic lamprophyre indicate that it can be regarded as a variety similar to aillikite, while other differences dominated by K-feldspar can be referred to damtjernite. According to Rb–Sr analysis, ultramafic lamprophyre dikes intruded at the turn of the Early and Middle Devonian, about 392 Ma ago. This directly proves the existence of Early Paleozoic alkali–ultramafic magmatism in the northern part of the southwest Siberian Platform. A finding of Devonian alkali–ultramafic lamprophyre is of dual predictive importance. On the one hand, it is indicative of the low probability of finding large diamond-bearing deposits in close association with aillikite. On the other hand, it can be indicative of a possible large Devonian diamond province in the studied territory, where diamondiferous kimberlite is structurally separated from aillikite.

DOI: 10.1134/S1075701516050068

INTRODUCTION

The aim of this work is to study ultramafic lamprophyre dikes in the Riphean–Vendian oil and gas deposits of the Irkineeva–Chadobets Trough within the Siberian Platform (SP), where they were identified for the first time in borehole cores at the Ilbokich gas–condensate deposit.

Most kimberlites and related rocks are Paleozoic and Mesozoic in age and are concentrated in the eastern part of the SP (Fig. 1). In the western part of the SP, in the north and center, there are a few Mesozoic kimberlite fields, while Mesozoic, Neoproterozoic, and Palaeozoic lamproite, kimberlite, and mafic lamprophyre occurrences are located in the extreme south (Pokhilenko et al., 2012). The complex of predictive criteria for commercial diamondiferous kimberlites and, primarily, mineralogical criteria based on the occurrence of low-Ca high-Cr pyrope in Carboniferous conglomerates, which is typical of Paleozoic diamond-rich kimberlite and is not observed in Mesozoic kimberlite, made it possible to identify the promising Tunguska Subprovince in the southwest SP, which covers the southwestern framing of the Tunguska Syneclise and Chadobets Elevation (Egorov, 2011; Dobretsov and Pokhilenko 2010; Dodin et al., 2008). However, no other ancient alkali–ultramafic magmatism features have been identified in the explored Tunguska Subprovince, except for Mesozoic carbonatite, alkali picrite, and alnoite at the Chadobets Elevation (Lapin, 2001; Lapin and Lisitsyn, 2004; Lapin and Pyatenko, 1992).

The discovery of the Ilbokich ultramafic lamprophyre occurrence—Middle Devonian aillikite—directly proves the existence of the Early Paleozoic stage of alkali–ultramafic magmatism in southwest SP within the explored Tunguska Subprovince.

This paper reports the results of geochronological, mineralogical, petrographical, and geochemical study of ultramafic lamprophyre, proves that they belong to aillikite, and discusses their implications for forecasting the diamond potential in the southwest SP.

GEOLOGICAL POSITION AND RESEARCH OBJECTS

The Ilbokich occurrence is located within the northern edge of the Irkineeva–Chadobets rift trough in the southwest SP. The Irkineeva–Chadobets Trough is a linear zone separating large lithospheric

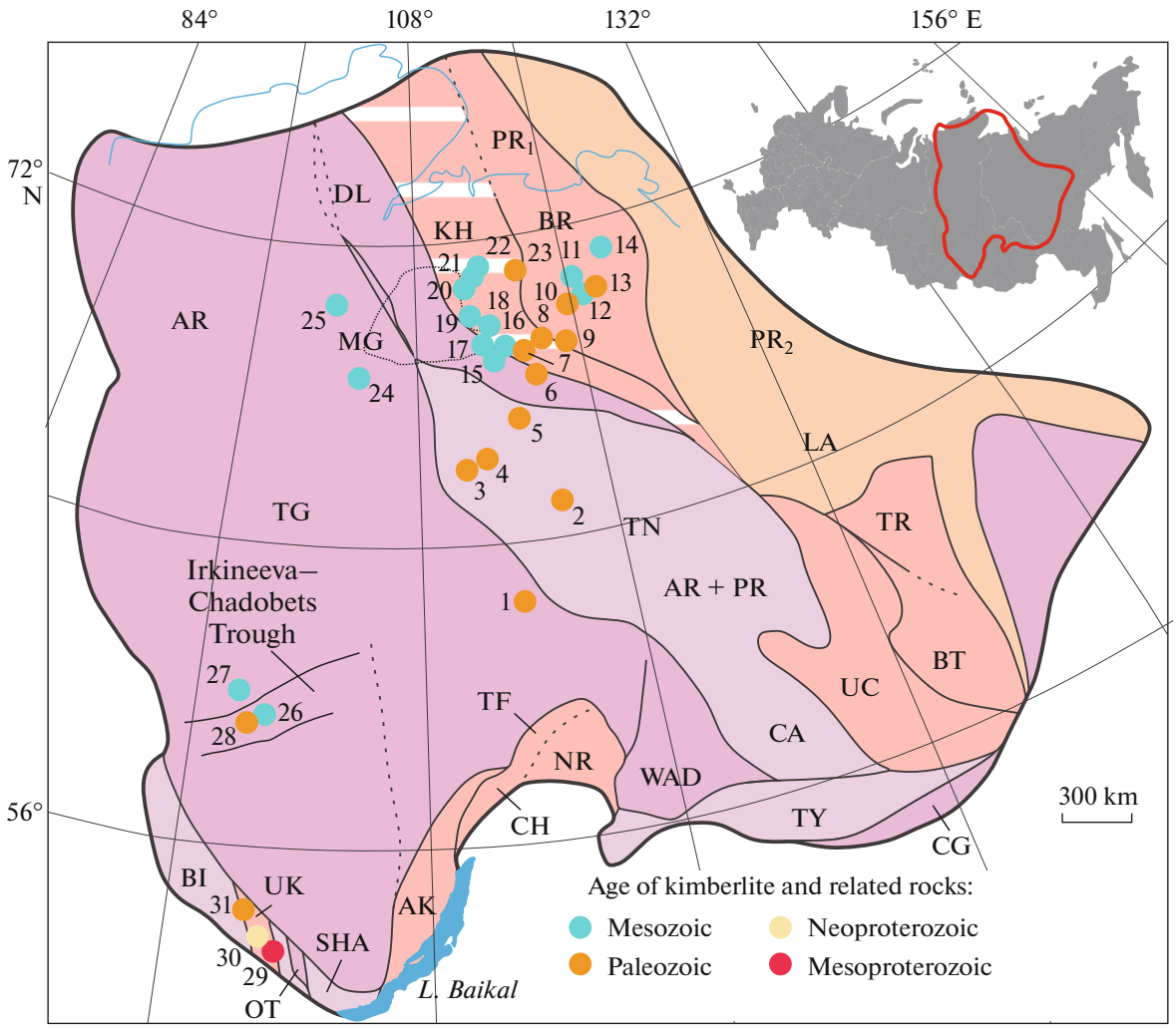

Fig. 1. Zoning of SP basement (Smelov and Timofeev, 2007) and position of kimberlite fields and related rocks according to (Zaitsev and Smelov, 2010; Pokhilenko et al, 2012; Kharkiv et al., 1998), and also national geological maps 1 : 1000000. Field numbers: (1) Minor Botuoba; (2) Nakyn; (3) Alakit–Markha; (4) Daldyn; (5) Upper Muna; (6) Chomurdakh; (7) Western Ukukit; (8) Eastern Ukukit; (9) Ogoner–Yuryakh; (10) Merchimden; (11) Kuoi; (12) Molodo; (13) Toluopka; (14) Khorbusuonka; (15) Kuranakh; (16) Luchakan; (17) Biriginda; (18) Dyuken; (19) Ary-Mastakh; (20) Starorechenskoe; (21) Orto-Iarga; (22) Ebelyakh; (23) Tomtor; (24) Kharamay; (25) Kotui (Dalbykh); (26) Chadobets; (27) Taigikun–Nemba; (28) Ilbokich area; (29) Ingash; (30) Zima Complex; (31) near-Sayan trough lamproitoids. Precambrian terranes: Western Aldan (WAD), Central Aldan (CA), Uchur (UC), Batomga (BT), Chogar (CG), Tynda (TY), Daldyn (DL), Khapchan (KH), Magan (MG), Akitkan (AK), Chuya (CH), Nechera (NR), Tonoda (TF), Sharyzhalgay (SHA), Onota (OT), Urik–Liy (UK), Biryusa (Bl), Tunguska (TG), Tyunga (TN), Birekte (BR), Tyryn (TR), and Lena–Aldan (LA).

blocks, which in terms of recent tectonics correspond to the Kama Arch in the north, Boguchany–Manzya in the south, and Angara–Lena with Nepa–Botuoba in the east (Fig. 2). This zone was identified for the first time by Yu.A. Kosygin in 1964 as a deep Riphean trough, which was confirmed by the Batolit and Altai–Severnaya Zemlya regional reference geophysical profiles and oil exploration seismic surveys by CDP seismic reflection methods (Staroseltsev, 2009). The Irkineeva–Chadobets Trough is composed of carbonate and terrigenous–carbonate sediments of the upper part of the Lower (?), Middle, and Upper Riphean with a total thickness of up to 8–10 km and is limited by major tectonic faults; high-amplitude inversion folded anticlinal uplifts—the Angara folding zone—formed in its marginal parts. In the Neo-Proterozoic, the trough was open to the Paleoasian Ocean, where the Altai–Sayan fold system is located today (Bush, 2009).

The large dome-shaped Chadobets Elevation (Fig. 3), which is one of the unique structures in the SP and 45 × 35 km in size, is located in the eastern part of the trough. The section of the elevation's sedimentary cover consists of Proterozoic, Paleozoic, and Mesozoic–Cenozoic deposits, as well as Triassic alkali–ultramafic rocks and gabbro–dolerite of the Siberian

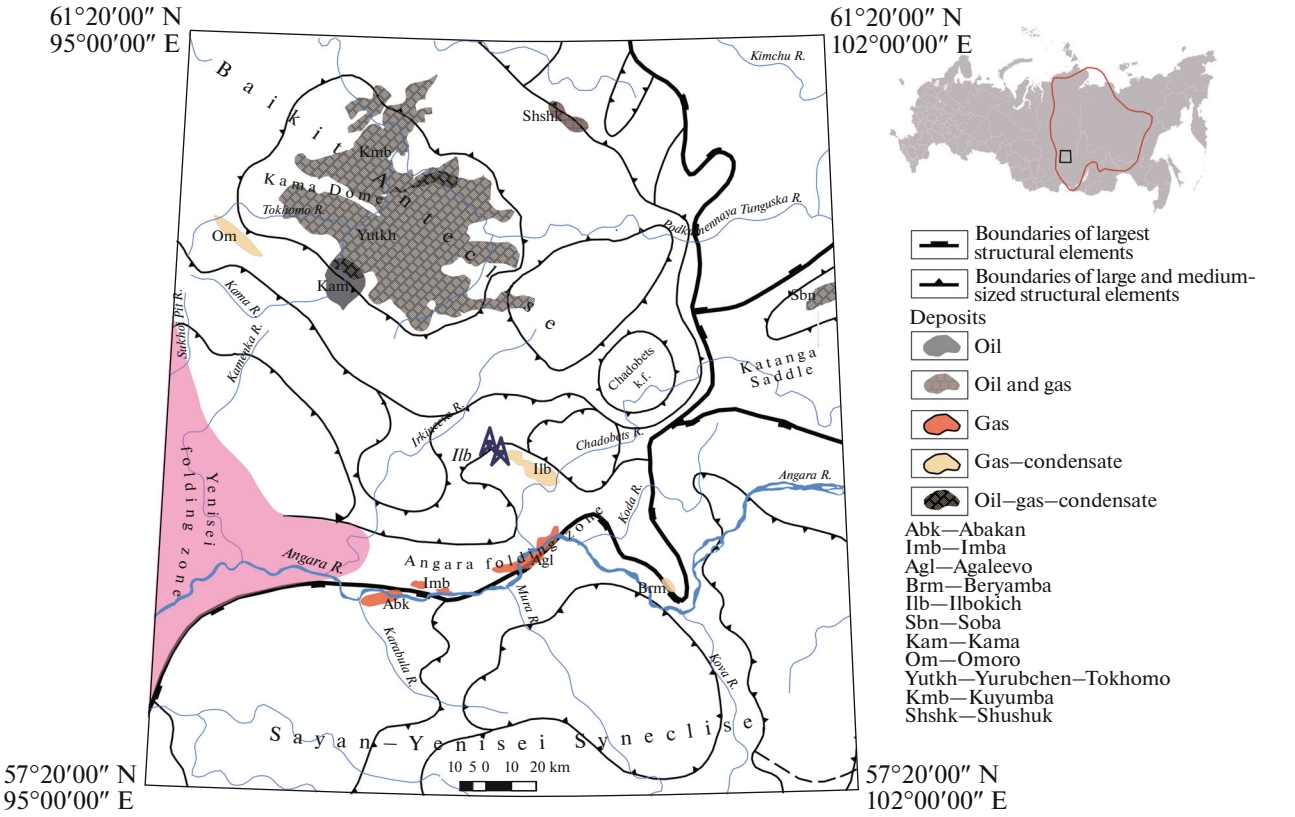

Fig. 2. Fragment of diagram of tectonic and oil-and-gas zoning in studied region (Kontorovich et al., 2009). *Ilb*—Ilbokichskaya boreholes 2 and 3.

Traps (Kirichenko et al., 2012; Lapin, 2001). In terms of tectonics, the Chadobets Elevation is an intersecting zone of two riftogenic structures, which is referred by some researches to the Angara–Kotui riftogenic trough (Staroseltsev, 2009).

This area was subject to thorough geological and geophysical studies, including many hundreds of kilometers of seismic profiles, dozens of deep boreholes drilled in oil and gas complexes of the sedimentary cover and, occasionally, in crystalline basement rocks. Large gas and gas–condensate deposits were identified here, such as the Abakan, Ilbokich, Agaleevo, Imba, etc. Along with carbonate and terrigenous rocks of the sedimentary cover, there are trappean intrusive bodies in a number of borehole sections.

Ultramafic lamprophyre dikes were found in borehole sections 2 and 3 within the Ilbokich area in the Chistyakovo deposits of the Riphean–Vendian Taseevo Group (Fig. 4). The host rocks are dominated by gray-colored or varicolored sand–aleurolite–clay varieties, and by dolomite formed under alluvial–deltaic plain and intertidal zone conditions.

The Ilbokichskaya-3 borehole core contains six levels of intruded ultramafic lamprophyres at depths of 2775–2833 m. The dikes are from 0.05 to 3.6 m in visible thickness. The contacts of these dikes are sharp, uneven, and subhorizontal (Fig. 4). The exocontacts are characterized by poorly defined crushing and carbonatization of host rocks. Narrow endocontact zones are distinguished by thin quenching zones and fine xenoliths of wall rocks. Eleven samples were subject to detailed petrographical investigations (Table 1).

RESEARCH METHODS

The mineral composition was studied by electron microprobe analysis (X-ray microanalysis) at the Laboratory for Mineral Substance Analysis at the Institute of Geology of Ore Deposits, Petrography, Mineralogy and Geochemistry, Russian Academy of Sciences, using a Jeol JXA-8200 electron probe microanalyzer equipped with five wave and one energy dispersive spectrometers. The analysis was carried out at an accelerating voltage of 20 kV, sample current of 20 nA, and probe diameter of 1–2 μm. The exposure time was 10 s for basic elements and 20–40 s for impurity elements. Corrections were made by the ZAF method using the JEOL software. Compounds similar in composition to the studied phases were used as standards for basic elements. The composition of olivine was studied by a precision procedure specified in (Sazonov et al., 2015).

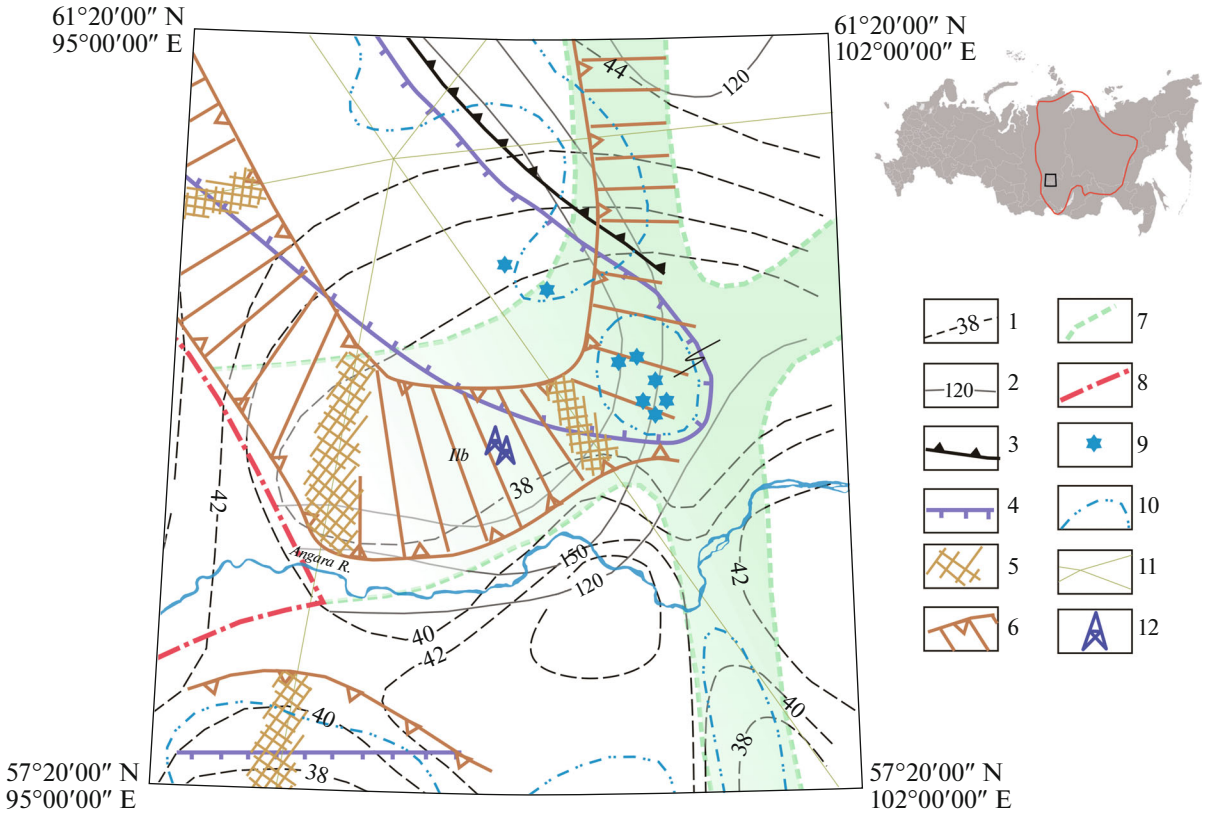

Fig. 3. Fragment of diagram of Chadobets Complex locations in southwestern SP with structural elements and physical properties of lithosphere, according to (Dashkevich, 1999). (1, 2) Structural contours: (1) Moho discontinuities, (2) asthenosphere roof; (3) boundary of conducting asthenosphere; (4) regional high-conductivity zones in earth's crust; (5, 6) complexly built sites of transition zone between earth's crust and mantle (crust–mantle mixture zones): (5) identified by deep seismic sounding; (6) forecasted; (7) boundaries of riftogenic structures (aulacogens, tectonomagmatic activation zones); (8) boundary of Yenisei tectonic belt and SP; (9) Mesozoic fields of kimberlite rocks; (10) diamond and/or pyrope identification areas in alluvium (or intermediate reservoirs); (11) profiles of deep seismic sounding and earthquake converted-wave method (Neftegeophizika Scientific Production Association); (12) boreholes uncovered ultramafic intrusions.

Concentrations of basic components of rocks were determined by *X-ray fluorescence analysis* (XRF) at the Institute of Geology of Ore Deposits, Petrography, Mineralogy and Geochemistry, Russian Academy of Sciences, using a Philips Analytical B.V. PW-2400 spectrometer. The agents were prepared to determine the rock-forming elements by melting 0.3 g of powder with 3 g of lithium tetroborate in an induction furnace. The accuracy of analysis was 1–5 rel. % for elements with concentrations of over 0.5 wt % and up to 12 rel. % for those with less than 0.5 wt %.

Detailed petrographical studies were conducted at the Laboratory for Local Research of Matter, Faculty of Geology, Department of Petrology, Moscow State University, using a Jeol JSM-6480LV raster scanning electron microscope (SEM) with an INCA-Energy 350 energy-dispersive analyzer. An acceleration voltage of 15 kV, current of 15 ± 0.1 nA, and mineral analysis locality of 4 μm were used. SEM images were obtained as BSE.

Minor and rare elements were determined by *mass spectrometry* with ICP-MS at the Institute of Microelectronics Technology and High Purity Materials, Russian Academy of Sciences. The rock samples were decomposed using inorganic acids in a sealed autoclave. Sample decomposition during chemical disintegration was controlled by addition of ^{161}Dy. The detection limits (DL) were 0.02–0.03 μg/g for REE, Hf, Ta, Th, and U; 0.03–0.05 μg/g for Nb, Be, and Co; 0.1 μg/g for Li, Ni, Ga, and Y; 0.2 μg/g for Zr; 0.3 μg/g for Rb, Sr, and Ba; and 1–2 μg/g for Cu, Zn, V, and Cr. The correctness of analysis was controlled by measuring standard samples GSP-2, BM, SGD-1A, and ST-1. The content determination error did not exceed 0.3% (±σ un.) for elements with up to 5*DL and 0.15% (±σ up.) for those with over 5*DL.

The Rb–Sr isotopic system of rocks and rock-forming minerals was studied at the Laboratory for Isotopic Geochemistry and Geochronology at the Institute of Geology of Ore Deposits, Petrography, Mineralogy and Geochemistry, Russian Academy of

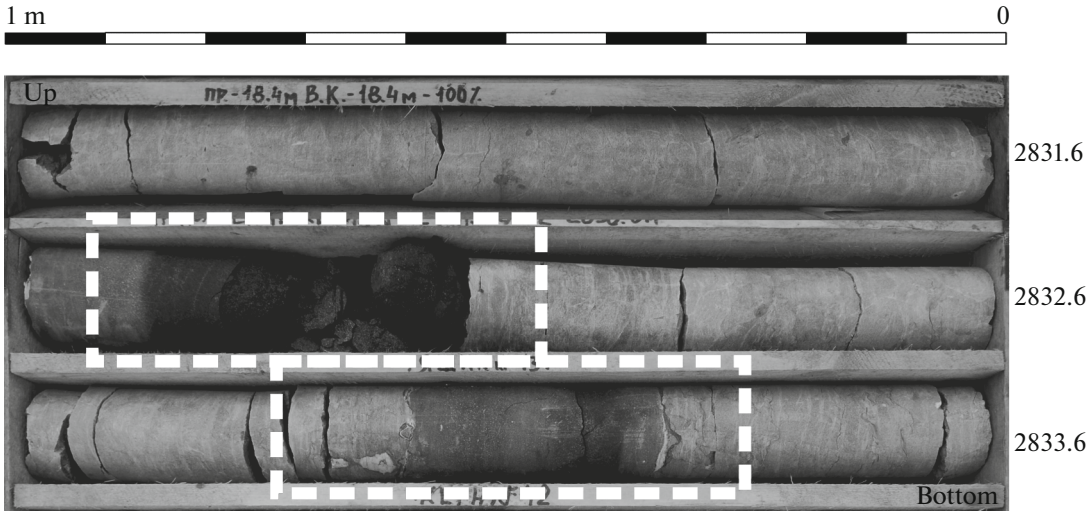

Fig. 4. Ultramafic intrusions and their contacts with host rocks in Ilbokichskaya-3 borehole.

Sciences, by common procedures for chemical preparation of samples for mass spectrometry analysis and by thermal ionization mass spectrometry.

The Rb and Sr contents in samples and $^{87}Rb/^{86}Sr$ were determined by isotopic dilution with a mixed $^{85}Rb–^{84}Sr$ tracer, which was added to samples just prior to chemical decomposition. Phlogopite and carbonate monofractions with 99% purity were selected. Weighed portions of about 0.05 g and 0.02 g were used in analyzing bulk phlogopite and carbonate samples, respectively. Chemical decomposition was carried out in sealed PFA-teflon vessels in a mixture of concentrated acids HF + HNO_3 (3 : 1) at atmospheric pressure and a temperature of 160°C throughout the day until complete dissolution of samples. Some studied phlogopite samples were pretreated with a 10% acetic acid solution for 1 h hour to remove carbonate phases. Weighed portions of carbonate minerals did not exceed 0.002 g. The procedure for their chemical preparation involved dissolving the sample in 6 M HCl at 120°C. Ion exchange chromatography was used to obtain pure Rb and Sr agents. The fractions were extracted in 2.4 M HCl using ion exchange columns filled with 3 mL of BioRad W50x8 cation exchanger with 200–400 mesh grains. The background contamination of the sample prepared with this procedure did not exceed 0.06 and 0.1 ng for Rb and Sr, respectively.

The Rb and Sr isotopic compositions of the extracted fractions were analyzed with a 54 Sector multicollector thermal ionization mass spectrometer (Micromass, United Kingdom). Correctness of the $^{87}Sr/^{86}Sr$ mass spectrometric measurements was controlled by systematic measurements of international standard of the Sr isotopic composition such as SRM-987. The $^{87}Sr/^{86}Sr$ error in the measured samples did not exceed 0.003% ($\pm 2\sigma$ un.). The error was at a level of 0.5% ($\pm 2\sigma$ un.) for $^{87}Rb/^{86}Sr$. The Rb–Sr age of the studied rocks was estimated by the isochronic construction method. In addition, common constant values were used to calculate the Rb–Sr age values (Steiger and Jäger, 1977).

RESULTS

Petrographical Description and Specific Features of the Mineral Composition

Ultramafic lamprophyres occur as homogeneous fine-grained massive rocks of dark greenish–gray color interspersed with equally spaced ore minerals.

The rock structure is porphyritic (Fig. 5). Olivine, more rarely, carbonate mineral phenocrysts are up to 1–1.5 mm in size (Figs. 5a, 6a, 7a). Phenocrysts are also observed as large crystals of perovskite replaced by ilmenite and rutile with a size up to 0.2 mm (Figs. 5a, 6a). The contents of phenocrysts vary from 5–10 to 25–35 vol % (Table 1) with prevailing rocks with 25 vol % of phenocrysts. In some samples (Ilb3-22-1), phenocrysts occur as alkali feldspar, which has a poikilitic appearance due to mica ingrowths. Some samples contain amphibole often intergrown with clinopyroxene (Ilb-28 and Ilb-24). The lamprophyre groundmass is fully crystalline; is characterized by a micrograined, hypidiomorphograined, heterogeneous structure; and consists of carbonate (predominant), fine laths of phlogopite, abundant segregations of perovskite partially replaced by rutile, ilmenite, sulfides (pyrite, pyrrhotite, chalcopyrite, and sphalerite), as well as spinel, fine grains of apatite, clinopyroxene, more rarely, amphibole and high-Ti garnet (Figs. 5–7). Most lamprophyres are occasionally characterized by an oriented structure due to abundant phlogopite laths, often identically oriented, immersed in granular carbonate. Carbonate minerals recrystallize on contact with host rocks.

Table 1. List of studied ultramafic lamprophyre samples from Ilbokichskaya-3 borehole with brief petrographical description

Sample	Sampling depth, m	Phenocryst composition	Groundmass composition
Ilb3-39	2775.3	5 vol %: Ol*	Ol, Phl, Cpx, Prv, Rt, Ap, ore minerals in Cb matrix
Ilb3-28	2817.8	25 vol %: major Ol, minor Cpx and Amp intergrowths	Phl, Cpx, Amp, Ilm, Prv, Spl, Ap, ore minerals in Cb matrix
Ilb3-24	2819.75	35 vol %: major Ol, minor Prv, Rt, Ap	Cb oikocrysts with ingrowths of Phl, Cpx, more rarely, Amp, Ilm, Spl, Prv, Rt and sulfides
Ilb3-27a	2825.5	25 vol %: Ol	Aggregate of Cb, Phl, Prv, Rt, Ap, Sph
Ilb3-27b		25 vol %: major Ol, minor Cb	Cb oikocrysts with ingrowths of Phl, Prv, Rt, Spl, Po, Ccp
Ilb3-22-1	2831.5	25 vol %: Ol, minor Cb, Fsp	Abundant Phl laths in Cb matrix with Prv, Rt and sulfide dissemination
Ilb3-22-2		35 vol %: Ol, minor Phl, Ap	Phl, Prv, Rt, Spl, Ap, Py, Po in Cb matrix
Ilb3-21	2832.8	25 vol %: Ol, minor Cb, Prv, Rt	Abundant Phl laths in Cb matrix with Spl, Ilm, Prv, Mag, Py
Ilb3-31 Ilb3-31/1 Ilb3-31/2	2817.35	Endocontact zone; rock consists of sites that vary in content of carbonate and silicate components; sites gradually replace each other. Silicate component is observed as small Ol phenocrysts immersed in Phl matrix with Ap, Ilm, Spl, Ttn ± Cb (sample Ilb3-31). matrix can contain relatively large round carbonate segregations. In sites dominated by carbonate component, silicate material is fragmented as rounded segregations and is evenly distributed in matrix of coarse-grained calcite aggregate (Ilb3-31/2).	

(Ol) olivine, (Phl) phlogopite, (Cpx) clinopyroxene, (Amp) amphibole, (Cb) carbonates, (Rt) rutile, (Spl) spinel, (Mag) magnetite, (Ilm) ilmenite, (Ap) apatite, (Prv) perovskite, (Ttn) titanite, (Py) pyrope, (Po) pyrrhotite, (Ccp) chalcopyrite, and (Fsp) alkali feldspar.
* Olivine in phenocrysts and groundmass is commonly altered and occurs as pseudomorphs of serpentine and carbonate minerals, except for sample Ilb3-28, containing preserved relics of unaltered mineral.

Olivine in phenocrysts and in the groundmass is commonly replaced by serpentine and calcite. Unaltered olivine was identified in sample Ilb-28. The contents of forsterite components (Fo) vary from 77.3 to 83.0 (Table 2) for considerable variations in NiO (0.07–0.40 wt %) and moderate variations in MnO (0.11–0.41 wt %), CaO (0.13–0.29 wt %), and TiO_2 (0.02–0.05 wt %). Olivine is characterized by a zoned structure (Fig. 7a). Marginal zones relative to central parts of crystals are characterized by an increased Fo content, higher NiO, Cr_2O_3, and a decrease in MnO content.

Clinopyroxene commonly forms small crystals (Fig. 6c), more rarely, single large intergrowths with amphibole (up to 0.150 mm). Clinopyroxene compositions form a continuous range from diopside to salite (Table 3) characterized by an increase in concentrations of Al_2O_3 (up to 2.67 wt %), TiO_2 (up to 3.24 wt %), FeO_{total} (up to 13.88 wt %), and Na_2O (up to 1.98 wt %) on a background of lower SiO_2, CaO concentrations and Mg# value (from 0.95 to 0.52), where Mg# = $Mg/(Mg + Fe^{2+})$ mol.

Amphibole is commonly observed in the groundmass, but most often as phenocrysts intergrown with clinopyroxene. It occurs as richterite (Mg# = 0.91–0.92), contains up to 1.57 wt % TiO_2 at 1.97 wt % K_2O and 6.1–8.1 wt % Na_2O (Table 3).

Garnet compositions correspond to the andradite–grossularite range with a high TiO_2 content. Garnet is characterized by a subeuhedral and anhedral form, often makes up sheath-shaped crystals, whose dimensions rarely exceed 100 μm; intergrowths with apatite; pyroxene; and phlogopite (Fig. 7b). Garnet is highly variable in TiO_2 with a content of from 2 to 17 wt % for up to 0.5 wt % Cr_2O_3 and up to 0.75 wt % ZrO_2 (Table 3).

Phlogopite is commonly observed as elongated zoned scales, more rarely, poikilitic crystals (Figs. 5, 6). In MgO, Al_2O_3, and FeO contents, the mica pertains to Al-rich phlogopite/biotite and is characterized by an intermediate composition between phlogopite, tetraferriphlogopite, eastonite (Al-rich phlogopite), and annite (Table 4; Figs. 8, 9). The central parts of zoned scales are enriched in Al_2O_3, MgO, BaO, and TiO_2 and are depleted in FeO with respect to marginal zones.

Spinel is abundant in the groundmass of the studied ores. Spinels include Ti-magnetite, magnetite, Cr-spinel and spinel differences with wide variations in the composition. Spinels are commonly characterized by

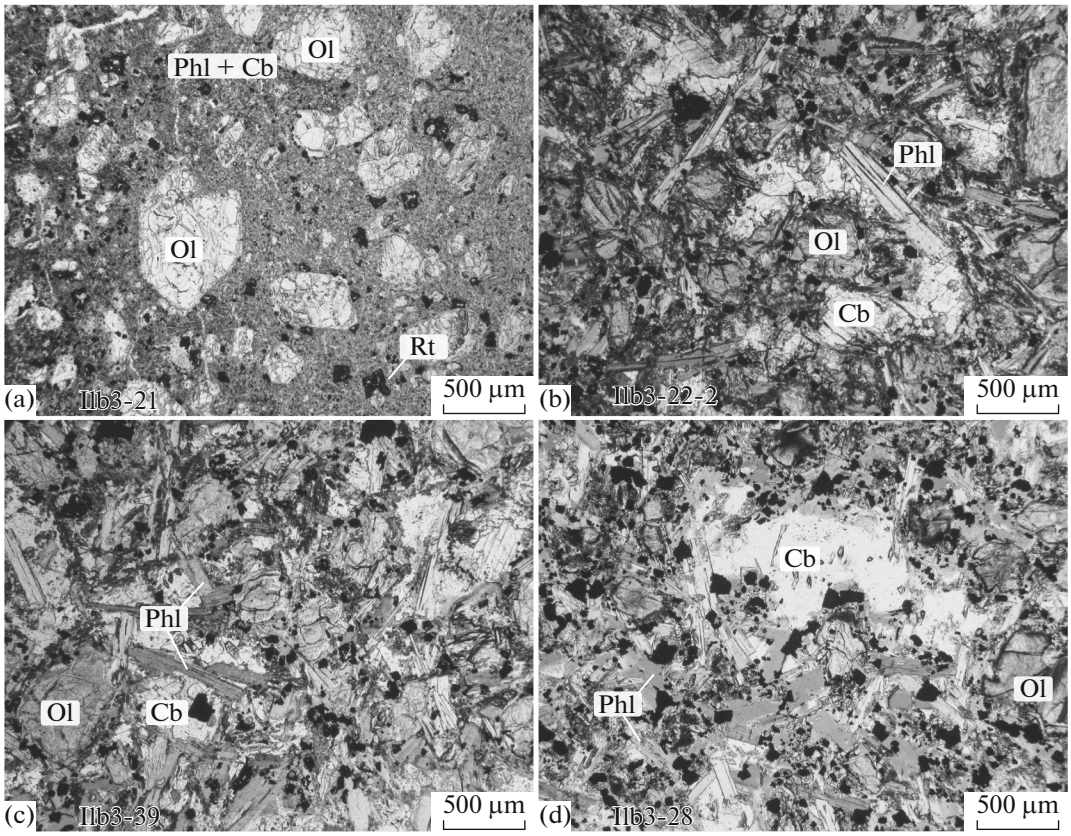

Fig. 5. Microphotographs of lamprophyre in transmitted light at one nicol. (Ol) Olivine, (Phl) phlogopite, (Cb) carbonates, and (Rt) rutile.

atoll-shaped crystals (50–10 μm), where the central zone consists of spinel or chrome–spinel and the outer framing is spinel or magnetite (Fig. 7b). In relations between Fe, Ti, Cr, Al, and Mg, spinels correspond to Ti-magnetite varieties (trend 2 after (Mitchell, 1995)) distinguished by an increase in Fe and Ti compared to a decrease in Mg, Al, and Cr (Table 5). The MgO content does not exceed 12.72 wt % (from 10.12 to 12.72 wt %), which together with a low Cr/(Cr + Al) ratio from 0.40 to 0.65, differentiates the studied spinel from that from orangeite and lamproite, according to (Mitchell, 1995).

Perovskite forms subphenocrysts of up to 0.2 mm in size and smaller segregations in the groundmass

Table 2. Representative compositions of olivine from sample Ilb3-28

No.	1	2	8	12	15	21	22	28	59	60
SiO_2	40.53	40.61	40.67	40.73	40.66	40.79	40.02	40.45	40.47	40.81
TiO_2	0.04	0.03	0.03	0.03	0.03	0.04	0.04	0.04	0.02	0.03
Al_2O_3	0.04	0.04	0.04	0.05	0.04	0.07	0.02	0.03	0.00	0.03
Cr_2O_3	0.05	0.07	0.07	0.05	0.07	0.05	0.02	0.05	0.02	0.08
FeO	11.91	10.30	11.11	11.02	9.87	10.79	13.39	12.25	11.72	10.52
MnO	0.14	0.12	0.12	0.12	0.12	0.12	0.20	0.15	0.41	0.12
MgO	47.45	48.32	48.32	48.32	48.73	48.41	46.26	47.23	47.86	48.60
CaO	0.19	0.14	0.14	0.14	0.15	0.14	0.29	0.18	0.13	0.15
NiO	0.26	0.39	0.32	0.38	0.40	0.38	0.15	0.22	0.07	0.39
Total	**100.61**	**100.01**	**100.82**	**100.81**	**100.07**	**100.78**	**100.40**	**100.59**	**100.68**	**100.72**
Fo, %	79.74	82.27	81.13	81.27	83.00	81.61	77.30	79.20	79.78	82.04

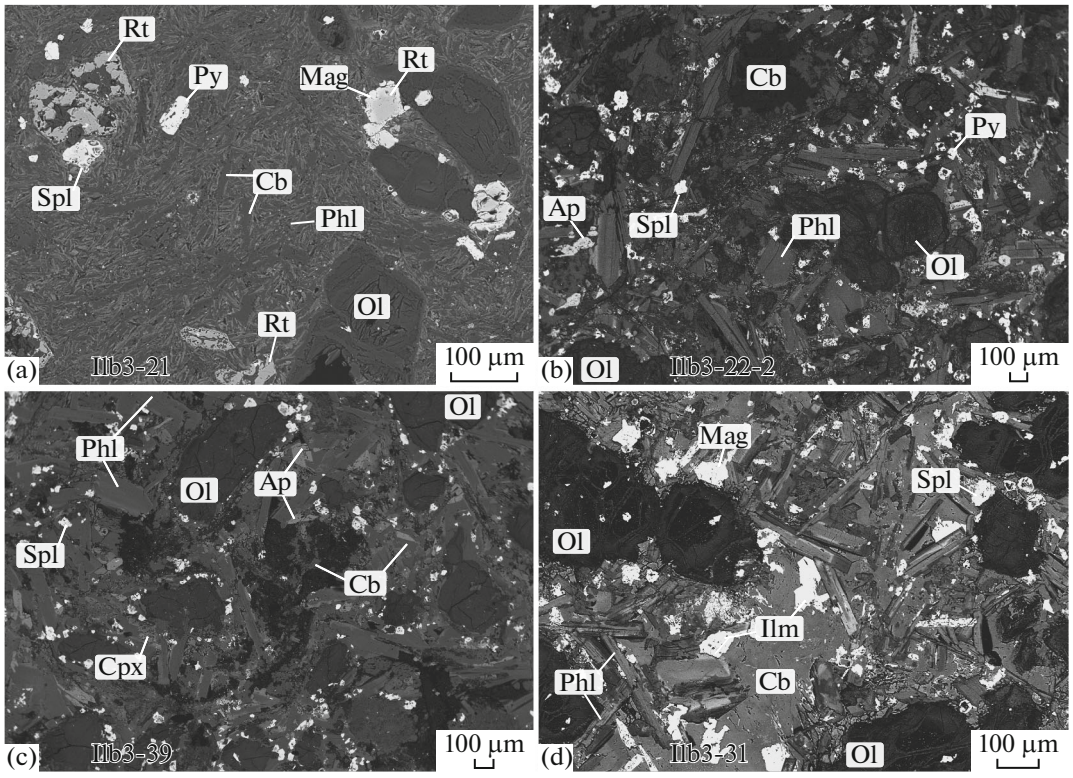

Fig. 6. Backscattered electron images of lamprophyre: (a) porphyritic rock structure; (b–d) specific features in groundmass composition. (Ol) olivine, (Cpx) clinopyroxene, (Phl) phlogopite, (Cb) carbonates, (Rt) rutile, (Spl) spinel, (Mag) magnetite, (Ilm) ilmenite, (Ap) apatite, and (Py) pyrope.

(0.04–0.06 mm), often intergrown with spinel. It is important to note the zoned replacement of perovskite by rutile and perovskite grain edges by ilmenite (Figs. 7c, 7d). Rutile is characterized by elevated Cr and Nb contents: 0.04–0.09 and 0.27–0.31 wt %, respectively (Table 5).

Apatite is characterized by relatively elevated concentrations of SrO (up to 0.9 wt %) and MnO (up to 0.04 wt %) (Table 6). The Cl–OH–F distribution in apatite is dominated by fluorine in the anion group, which is typical of apatite from carbonatites (Patiño Douce et al., 2011).

Carbonate minerals represent a continuous range between calcite, ankerite, and dolomite (Table 7). The earliest phenocrysts are predominantly calcitic in composition, while carbonates from the groundmass are enriched in MgO (up to 16 wt %) and FeO (up 17 wt %).

Chemical Composition

Representative compositions of the ultramafic lamprophyre from Ilbokichskaya-3 borehole are given in Table 8.

Major oxides. Variations in the concentrations of rock-forming petrogenic oxides (Fig. 10; Table 8), especially SiO_2, MgO, and CaO, are related to variations in the contents of carbonate and silicate components: an increase in the CaO content results in a decrease in the SiO_2 and MgO concentrations. The studied rocks are characterized by moderate Mg# values (0.68–0.81), which differentiates them from typical kimberlite and alkali-like picrite and ultramafic lamprophyre, such as aillikite (Tappe et al., 2006). The studied rocks are also distinguished by enrichment in K_2O (2.22–3.73 wt %) and TiO_2 (2.53–4.32 wt %).

Minor elements. The distribution spectra of rare and rare-earth elements normalized to the primitive mantle and chondrite C1, respectively, (Fig. 11) correspond to the spectra of ultramafic lamprophyres: they are characterized by incompatible elements, the presence of a poorly defined negative Zr–Hf anomaly, and the absence of negative Nb–Ta, K, and Ti anomalies on a background of moderate fractionation of rare earth elements ($(La/Yb)_n$ = 37–62).

Rb–Sr Isotopic Age

Sample Ilb3-28 was selected for geochronological studies based on petrographical observations and the specific features of its mineral composition. It has no

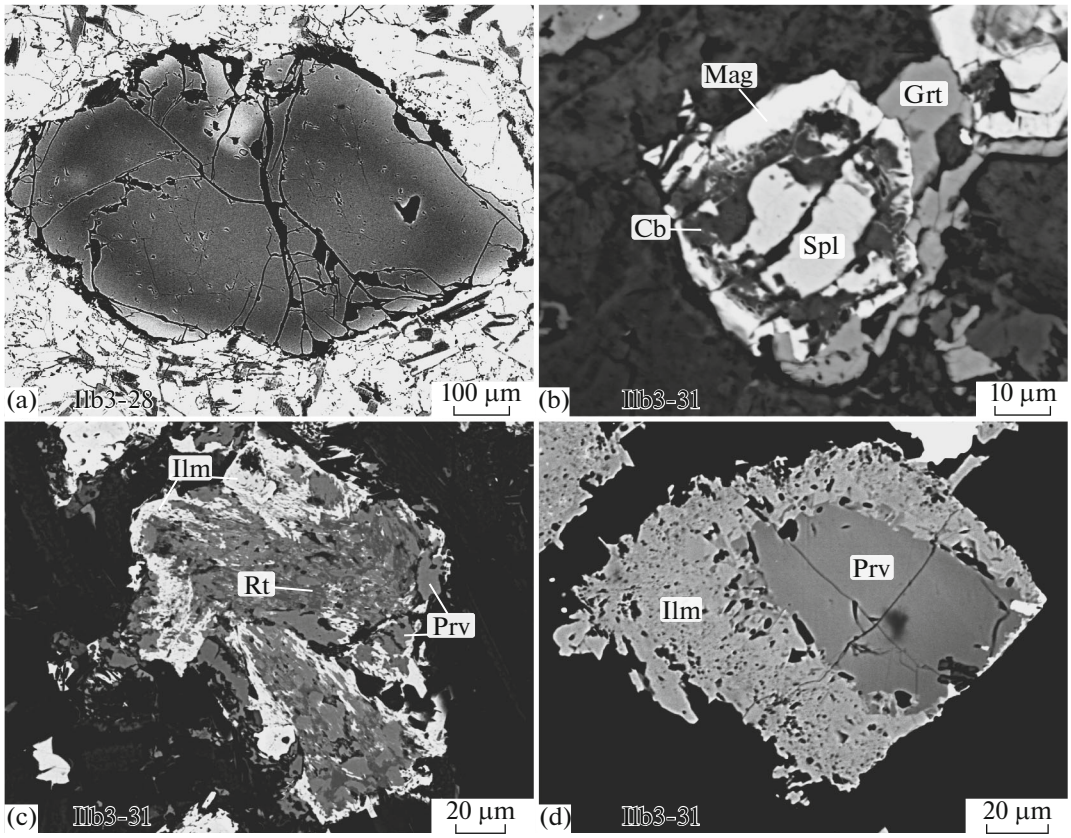

Fig. 7. Backscattered electron images of lamprophyre minerals: (a) zoned olivine crystal; (b) atoll-shaped spinel crystals; (c) perovskite subphenocrystal (light grey) replaced by rutile (dark grey) and ilmenite; (d) perovskite crystal from groundmass replaced by ilmenite. (Cb) Carbonates, (Grt) garnet, (Ilm) ilmenite, (Mag) magnetite, (Prv) perovskite, (Rt) rutile, and (Spl) spinel.

traces of marginal interaction with the host rocks (recrystallization, quenching, etc.) and is the least affected by secondary alterations. The rock is porphyritic in structure (Fig. 5d). Phenocrysts making up about 25% of the rock occur as fresh olivine or euhedral serpentine pseudomorphs after olivine with a size of 200 × 500 μm, more rarely, as clinopyroxene intergrown with richterite laths. It is mostly poikilitic in appearance: ingrowths of mica, clinopyroxene, amphibole and segregations of ilmenite (+ perovskite), spinel, apatite, and sulphides (pyrrhotite) occur on the background of the carbonate matrix.

The Rb–Sr data (Table 9) obtained for the bulk sample and rock-forming minerals (six points in total) were plotted in the correlation diagram (Fig. 12). The experimental points in the diagram form a single linear relation, the slope of which corresponds to the age of 391.7 ± 1.9 Ma. The relatively low mean square weighted deviation (MSWD) of 6.1, characterizing the dispersion of points with respect to the approximating line, indicates that the relation of points observed on the diagram is almost isochronous.

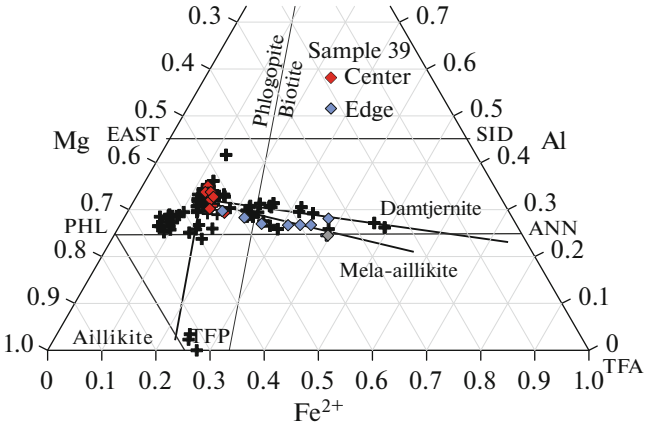

Fig. 8. Mica composition (atomic number) in Al–Mg–Fe_{total} (Fe^{2+}) system from ultramafic lamprophyre (black crosses) of Ilbokichskaya-3 borehole. (PHL) Phlogopite, (EAST) eastonite, (ANN) annite, (SID) siderophyllite, (TFP) tetraferriphlogopite, and (TFA) tetraferriannite.

Table 3. Representative compositions of clinopyroxene, amphibole, and garnet from ultramafic lamprophyre of Ilbokichskaya-3 borehole

Sample	Ilb3-39		Ilb3-28				Ilb3-28		Ilb3-31			
mineral	Cpx	Cpx	Cpx	Cpx	Cpx	Cpx	Amp	Amp	Grt	Grt	Grt	Grt
zone	core	edge	core*				core*		core*			
SiO_2	50.80	48.94	54.82	50.63	52.48	52.90	55.53	54.37	35.55	31.93	29.71	32.15
TiO_2	1.14	1.42	0.20	0.91	0.83	0.44	1.01	0.6	1.91	8.16	14.75	9.81
ZrO_2	–	–	–	–	–	–	–	–	–	–	0.7	0.2
Al_2O_3	1.92	2.71	0.00	2.37	1.58	0.65	0.42	0.91	3.03	1.68	1.4	1.28
Cr_2O_3	0.01	0.02	0.11	0.00	0.00	0.00	0.00	0.06	–	0.44	–	–
FeO_t	5.51	12.53	1.52	6.28	5.47	3.75	2.49	8.62	24.1	22.83	20.09	21.17
MnO	0.17	0.28	0.00	0.22	0.17	0.12	0.00	0.00	0.11	0	0.23	0.15
MgO	14.70	9.63	17.45	14.21	15.24	16.14	22.45	18.52	0.86	1.16	1.22	1.65
CaO	24.68	22.35	25.39	24.38	24.68	25.19	7.18	3.71	33.38	32.84	31.98	33.122
Na_2O	0.38	1.36	0.27	0.42	0.45	0.16	5.51	8.13	–	–	0.23	0.08
K_2O	0.02	0.05	0.00	0.00	0.00	0.00	1.97	0.56	–	–	–	–
Total	99.32	99.28	99.76	99.42	100.90	99.35	96.56	95.48	98.95	99.05	100.29	99.58
Mg#	0.83	0.58	0.95	0.80	0.83	0.88	0.92	0.87	0.06	0.08	0.10	0.12

* Analysis data in wt % of oxides recalculated to 100%.

Table 4. Representative compositions of mica from ultramafic lamprophyre of Ilbokichskaya-3 borehole

Sample	Ilb3-39								Ilb3-22-2			Ilb3- 22-1			Ilb3-31-2		
zone	core	edge	core	edge	core	edge	core*	core*	core*	core*	core*	core*	core*	core*	core*	core*	core*
SiO_2	35.94	37.01	36.67	36.90	35.44	37.38	36.05	37.31	35.85	36.54	36.93	35.53	36.45	35.64	40.10	40.04	39.77
TiO_2	4.52	4.11	3.62	3.38	4.49	3.61	4.36	3.16	4.23	4.17	4.07	5.89	5.31	5.50	0.46	0.43	0.58
Al_2O_3	15.21	11.44	13.19	10.05	15.20	11.13	14.61	11.27	15.92	14.93	15.27	13.30	13.38	13.30	13.94	13.10	14.24
FeO_t	8.41	21.70	9.15	22.83	7.77	19.50	8.97	20.95	7.87	7.99	7.69	15.54	15.71	14.16	4.48	6.44	5.56
MnO	0.09	0.10	0.12	0.29	0.07	0.23	0.08	0.27	0.03	0.06	0.07	0.17	0.17	0.15	0.11	0.37	0.13
MgO	18.90	10.93	18.94	11.61	19.17	13.11	18.66	12.62	19.49	19.59	19.50	14.22	14.93	15.13	25.09	23.97	24.46
CaO	0.08	0.18	0.03	0.09	0.06	0.19	0.08	0.22	0.04	0.11	0.07	0.09	0.26	0.21	0.08	0.12	0.14
BaO	1.14	0.13	0.27	0.00	1.35	0.00	0.49	0.00	1.43	0.34	0.33	0.48	0.29	0.48	–	–	–
Na_2O	0.20	0.12	0.13	0.13	0.21	0.19	0.11	0.16	0.18	0.22	0.21	0.23	0.21	0.21	0.19	0.23	0.22
K_2O	9.86	9.98	8.99	9.80	8.98	9.98	9.39	9.94	9.66	10.07	9.87	9.88	9.39	9.59	10.36	10.25	10.46
F	0.75	0.35	0.75	0.38	0.73	0.29	0.65	0.27	0.70	0.70	0.71	0.60	0.44	0.55	0.19	0.00	0.27
Total	95.15	96.35	91.86	95.47	93.47	95.78	93.45	96.24	95.40	94.74	94.73	95.93	96.53	94.92	95.00	94.95	95.83

* Core of unzoned grain.

We consider the Rb–Sr dating of about 392 Ma as a geologically significant date corresponding to the rock age, because:

(1) the Rb–Sr geochronological investigation has been carried out for a sample devoid of petrographical features of imposed alterations using five mineral fractions and one bulk sample;

(2) the obtained linear relation of points in the Rb–Sr diagram is similar to the isochronous type in its statistical parameters, primarily in the MSWD value;

(3) the low initial isotopic ratio of $^{87}Sr/^{86}Sr$ = 0.7033 is consistent with the mantle genesis of the studied rocks;

(4) the resulting estimate of the time of ultrabasic magmatism does not contradict the geological position of dikes.

Hence, it is assumed that the ultramafic lamprophyre dikes intruded at the turn of the Early and Late Devonian, about 392 Ma ago (Cohen et al., 2013).

Table 5. Representative compositions of spinelide and rutile from ultramafic lamprophyre of Ilbokichskaya-3 borehole

Sample	Ilb3-21	Ilb3-21	Ilb3-24	Ilb3-24	Ilb3-22-2	Ilb3-31	Ilb3-21	Ilb3-21
mineral	Spl	Spl	Spl	Spl	Spl	Spl	Ru	Ru
SiO_2	0.10	0.04	0.14	0.11	0.06	0.04	0.02	0.01
TiO_2	4.58	13.46	4.29	10.77	12.63	11.43	98.17	98.31
ZrO_2	–	–	–	–	–	–	0.03	0.12
SnO_2	–	–	–	–	–	–	0.00	0.01
Al_2O_3	14.63	7.59	16.51	9.67	8.56	7.50	0.00	0.01
Cr_2O_3	38.38	13.62	39.56	19.73	11.52	8.06	0.04	0.09
V_2O_5	0.25	0.25	0.24	0.25	0.15	0.15	–	–
FeO_t	29.70	52.95	25.97	45.60	53.36	62.78	0.28	0.33
MnO	0.28	0.37	0.35	0.43	0.42	0.53	–	–
MgO	11.87	11.24	12.72	12.48	12.32	10.12	0.01	0.01
NiO	0.13	0.18	0.16	0.16	0.11	0.21	–	–
ZnO	0.06	0.04	0.10	0.06	0.04	0.04	–	–
Nb_2O_5	–	–	–	–	–	–	0.31	0.27
Ta_2O_5	–	–	–	–	–	–	0.03	0.01
WO_3	–	–	–	–	–	–	0.02	0.04
Total	99.97	99.73	100.01	99.26	99.19	100.84	100.84	100.84

Table 6. Representative compositions of apatite from ultramafic lamprophyre of Ilbokichskaya-3 borehole

Sample	Ilb3-22-2	Ilb3-22-2	Ilb3-22-2	Ilb3-22-2	Ilb3-31	Ilb3-31	Ilb3-39	Ilb3-24
SiO_2	0.65	1.40	1.18	1.29	1.00	1.17	1.72	1.34
TiO_2	0.01	0.00	0.05	0.05	0.04	0.00	0.09	0.13
Al_2O_3	0.01	0.00	0.02	0.00	0.01	0.00	0.02	0.01
La_2O_3	0.13	0.04	0.00	0.05	0.05	0.08	0.00	0.09
Ce_2O_3	0.16	0.08	0.02	0.05	0.10	0.02	0.03	0.20
FeO_t	0.62	0.14	0.20	0.17	0.16	0.07	0.10	0.25
MnO	0.02	0.01	0.02	0.00	0.00	0.00	0.04	0.00
MgO	0.06	0.08	0.02	0.10	0.03	0.05	0.08	0.09
CaO	50.94	52.24	53.25	53.02	52.95	53.62	53.68	53.01
BaO	0.05	0.00	0.00	0.04	0.00	0.00	0.00	0.00
SrO	0.88	0.38	0.47	0.35	0.60	0.43	0.37	0.42
Na_2O	0.77	0.11	0.12	0.07	0.14	0.10	0.11	0.31
P_2O_5	37.82	37.80	38.67	38.17	40.42	40.26	35.05	35.55
F	1.46	1.15	1.68	1.25	1.60	1.71	1.13	1.19
Cl	0.09	0.06	0.03	0.06	0.04	0.03	0.07	0.06
SO_3	0.18	0.25	0.12	0.26	0.08	0.11	0.28	0.19
Total	93.21	93.23	95.12	94.39	96.55	96.92	92.25*	92.30*

* Amount minus proportion of oxygen replaced by F and Cl.

Table 7. Representative compositions of carbonate from ultramafic lamprophyre of Ilbokichskaya-3 borehole

Sample	Ilb3-22-2		Ilb3-22-1				Ilb3-31/2	Ilb3-21				
zone	center	edge	g.m.	g.m.	g.m.	phen.	phen.	g.m.	g.m.	center	edge	edge
FeO t	0.29	5.14	0.28	2.41	9.28	0.96	0.33	5.95	17.45	5.13	7.64	11.86
MnO	0.34	0.49	0.00	0.22	0.57	0.30	0.06	0.24	0.14	0.12	0.30	0.38
MgO	0.22	16.27	0.04	3.73	13.97	0.41	0.09	13.23	8.76	13.59	4.93	9.67
CaO	56.48	29.82	56.49	48.11	29.38	54.17	55.97	32.06	27.70	33.14	39.37	32.16
CO_2	42.67	48.28	43.19	45.53	46.81	44.16	43.55	48.52	45.94	48.03	47.76	45.93
Total	100.00	100.00	100.00	100.00	100.00	100.00	100.00	100.00	100.00	100.00	100.00	100.00

(phen.) phenocryst, (g.m.) groundmass.

DISCUSSION

Classification Problems of the Studied Rocks

Dikes from the Ilbokichskaya-3 borehole section belong to the ultramafic lamprophyre family. Rocks of this family, first, are very rare and, second, are distinguished by wide variations in mineral composition. Due to this, their petrological–mineralogical classification is very complicated and has not been fully developed (Bogatikov et al., 2009). The studied rocks were identified using the classification procedures for ultramafic lamprophyre proposed by (Tappe et al., 2005). As a result, the studied rocks were referred to aillikite and damtjernite taking into account the specific features in their mineral and chemical compositions.

According to (Tappe et al., 2005), *aillikite* is a carbonate-rich lamprophyre composed of olivine and phlogopite phenocrysts immersed in groundmass comprising olivine, phlogopite, primary carbonate, spinel, ilmenite, rutile, perovskite, apatite, and Ti-rich garnet. *Damtjernite* is lamprophyre enriched in feldspathoids and/or feldspar, consisting of olivine, phlogopite, and clinopyroxene phenocrysts immersed in the groundmass with phlogopite–biotite, clinopyroxene, spinel, ilmenite, rutile, perovskite, Ti-rich garnet, titanite, apatite, primary carbonate, and minor nepheline.

In addition to the general petrographical features and mineral composition, the similarity of Ilbokich ultramafic lamprophyre to aillikite is also confirmed by the specific features in the chemical composition of minerals. Olivine differs in the content of Fo component (Table 2) from typical olivine from kimberlite and lamproite characterized by higher Fo contents in general (Mitchell, 1995; Prelevic et al., 2005; Sazonova et al., 2015); however, it is similar in this parameter (Mg# = 90–76) to olivine from Labrador ultramafic lamprophyre (aillikite–damtjernite) (Tappe et al., 2006, 2008). The evolution of clinopyroxene compositions expressed in higher Al_2O_3, TiO_2, FeO_{total}, and Na_2O concentrations on a background of lower SiO_2,

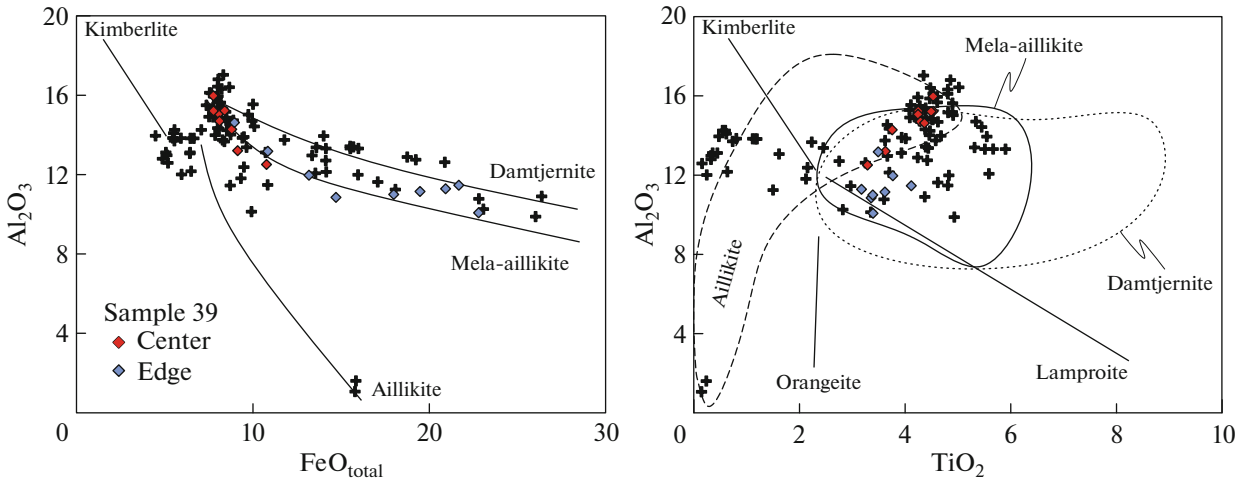

Fig. 9. Al_2O_3–FeO_{total} and Al_2O_3–TiO_2 (wt %) diagrams for mica. Fields and trends according to (Mitchell, 1995; Tappe et al., 2006). See legend in Fig. 8.

Table 8. Representative compositions of ultramafic lamprophyre from Ilbokichskaya-3 borehole

Sample	Ilb3-24	Ilb3-21	Ilb3-31a	Ilb3-28	Ilb3-27a	Ilb3-27b	Ilb3-22-2	Ilb3-31b	Ilb3-39
SiO_2	34.63	28.51	32.38	31.54	27.87	26.77	33.33	24.1	32.62
TiO_2	4.32	4.2	3.81	4.32	4.1	3.37	4.03	2.53	3.95
Al_2O_3	3.62	4.44	4.89	3.72	5.49	3.67	5.01	3.21	4.71
Fe_2O_{3t}	10.86	10.66	10.78	11.48	10.06	9.82	11.54	7.14	11.56
MnO	0.194	0.146	0.172	0.153	0.168	0.189	0.147	0.126	0.173
MgO	16.51	13.88	18.7	20.27	10.73	13.18	14.94	15.47	16.46
CaO	12.52	15.12	12.78	12.13	14.8	15.54	12.19	22.04	13.45
Na_2O	0.95	0.3	0.32	0.7	0.27	0.22	0.44	0.24	0.42
K_2O	2.51	2.22	3.35	3.2	3.73	2.62	3.03	2.53	3.08
P_2O_5	0.45	0.63	0.78	0.51	0.75	0.51	0.63	1.04	0.68
LOI	12.37	19.01	11.13	10.57	20.64	21.78	13.91	20.51	12.1
Total	**98.93**	**99.12**	**99.09**	**98.59**	**98.61**	**97.67**	**99.20**	**98.94**	**99.20**
Li	80.03	88.32	101.09	20.60	58.84	50.07	62.96	64.55	75.25
Be	1.55	1.85	1.97	2.49	1.74	1.22	1.84	2.27	2.03
Sc	20.98	23.48	25.71	20.59	25.62	19.48	28.99	14.06	29.22
V	150	148	215	223	158	106	202	155	201
Cr	926	719	710	826	625	588	638	472	596
Co	70	66	57	59	45	38	58	35	59
Ni	738	692	576	736	481	483	588	392	522
Cu	93	118	109	98	135	99	139	63	134
Zn	85	77	92	67	214	126	77	52	105
Ga	11.96	13.34	14.67	11.80	14.43	10.67	14.85	11.95	14.29
Rb	85.78	81.62	113.79	89.64	110.63	76.85	125.34	84.50	123.31
Sr	936.71	961.48	1364.84	1537.41	564.16	943.15	1044.12	3975.34	1139.33
Y	17.22	16.91	21.14	12.14	17.15	13.99	19.13	12.63	18.32
Zr	263.88	303.10	312.82	267.68	323.20	269.04	384.87	173.15	364.19
Nb	101.03	95.14	118.37	92.20	99.92	82.69	109.05	74.22	114.50
Mo	0.49	3.16	0.45	1.28	2.07	2.75	0.92	0.94	4.16
Ba	976.82	890.22	1425.42	1039.35	995.75	862.13	1335.17	676.07	1363.19
La	91.21	69.82	80.81	49.56	63.48	58.65	72.36	59.22	69.34
Ce	190.23	142.80	156.99	104.82	128.61	117.77	143.61	117.92	137.07
Pr	22.69	17.39	19.01	13.35	15.55	14.58	17.42	12.47	16.33
Nd	89.48	67.91	72.59	52.05	60.13	56.53	68.09	48.64	64.32
Sm	13.95	10.78	11.39	8.43	9.84	8.82	10.73	7.54	10.24
Eu	3.42	2.93	3.10	2.31	2.91	2.48	2.91	1.95	2.63
Gd	9.59	7.98	8.65	6.13	7.45	6.56	8.16	5.45	7.90
Tb	1.20	0.99	1.12	0.77	0.95	0.84	1.05	0.68	1.03
Dy	4.70	4.16	4.76	3.06	4.06	3.42	4.53	2.75	4.41
Ho	0.72	0.68	0.78	0.48	0.67	0.56	0.72	0.44	0.74
Er	1.62	1.58	1.93	1.14	1.65	1.32	1.84	1.07	1.81
Tm	0.18	0.19	0.23	0.13	0.19	0.16	0.22	0.13	0.21
Yb	1.05	1.07	1.34	0.81	1.14	0.92	1.30	0.77	1.34
Lu	0.13	0.15	0.17	0.11	0.16	0.12	0.17	0.09	0.18
Hf	6.95	8.19	7.98	6.92	8.86	6.84	9.45	4.23	9.71
Ta	7.67	6.04	7.08	7.06	6.08	5.60	5.00	3.65	6.40
Th	9.50	6.51	7.39	4.50	5.87	5.40	7.12	5.68	6.59
U	2.17	1.78	1.96	0.91	1.96	1.71	2.14	1.47	2.10
Pb	10.66	6.50	5.64	6.36	16.48	18.61	5.12	9.49	23.59

Concentrations of petrogenic oxides, Cr, Co, Ni, Cu, Zn, according to XRF data; concentrations of other elements, according to ICP-MS data.

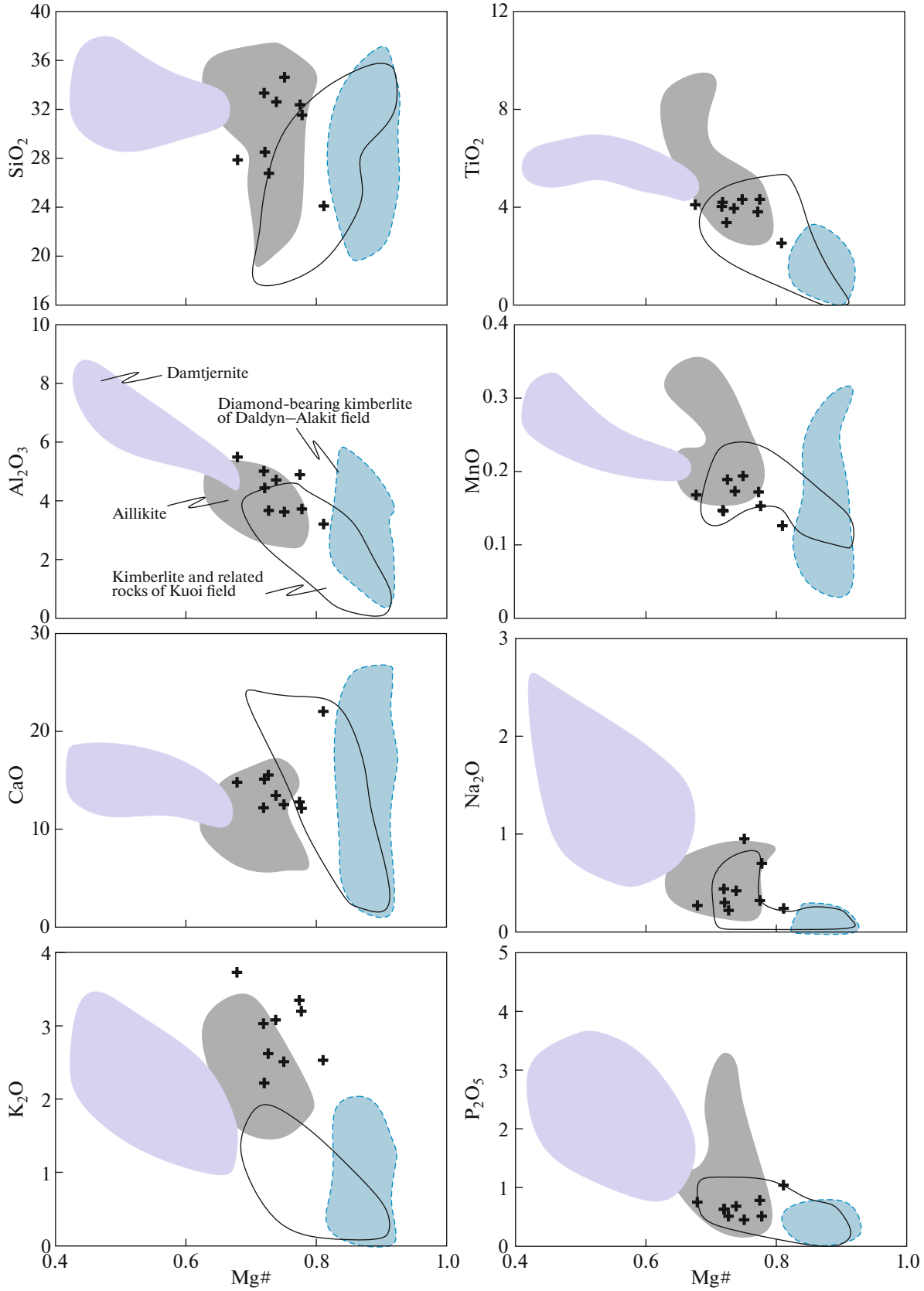

Fig. 10. Diagrams of oxide concentration (wt %) and Mg# for studied rocks in Ilbokichskaya-3 borehole (black crosses). Aillikite and damtjernite fields according to (Tappe et al., 2006; Tappe et al., 2008). Fields of kimberlites and related rocks in Yakut diamondiferous province, according to (Bogatikov et al., 2004; Kargin et al., 2011) and author's unpublished data.

CaO concentrations and Mg# value (Table 3) is also more typical of aillikite (Tappe et al., 2006) than of other ultramafic alkali rocks.

The position of figurative points for phlogopite in the Al_2O_3–FeO_{total} and Al_2O_3–TiO_2 diagrams (Fig. 9) is the most comparable with the field of mica from ultramafic lamprophyre with an aillikite–carbonatite composition (aillikite and damtjernite, according to (Tappe et al., 2006)). The elevated Al_2O_3 content makes it impossible to compare the studied mica with phlogopite from orangeite or lamproite according to (Mitchell, 1995).

The calculation of HF and H_2O activities in the fluid log(fHF/fH_2O), being in equilibrium with apatite from the studied rocks (Tacker and Stormer, 1989), at 1000°C yields values in the range from –3.6 to –4.4. These data are consistent with the relation of fluorine and water activities at given T in the fluid, being in equilibrium with aillikite and glimmerite (Tappe et al., 2006).

The chemical composition of the rocks also indicates that they correspond to aillikite. In the binary diagrams of bulk sample compositions, figurative points of the studied rocks are comparable with aillikite fields (Fig. 10). Meanwhile, it should be noted that in terms of concentrations of petrogenic elements not related to phlogopite, the figurative points of the studied rocks are also overlapped by regions with compositions of Mesozoic kimberlite–alkali picrite/lamprophyre at the Kuoi field in the northeast SP. Ilbokich dikes differ by a higher Mg# from typical damtjernite of the Labrador Province (Tappe et al., 2006) with a high K-feldspar content in the groundmass and by a lower Mg# (Fig. 10) from diamond-bearing kimberlite of the Yakut Province (Kargin et al., 2011). The distribution of rare and rare-earth elements in the multielement diagrams (Fig. 11) is comparable to the most depleted varieties of Labrador aillikite (Tappe et al., 2006).

Hence, specific features in the mineral and chemical compositions of the studied ultramafic lamprophyres make it possible to identify them as similar to aillikite, while some varieties can be referred to damtjernite.

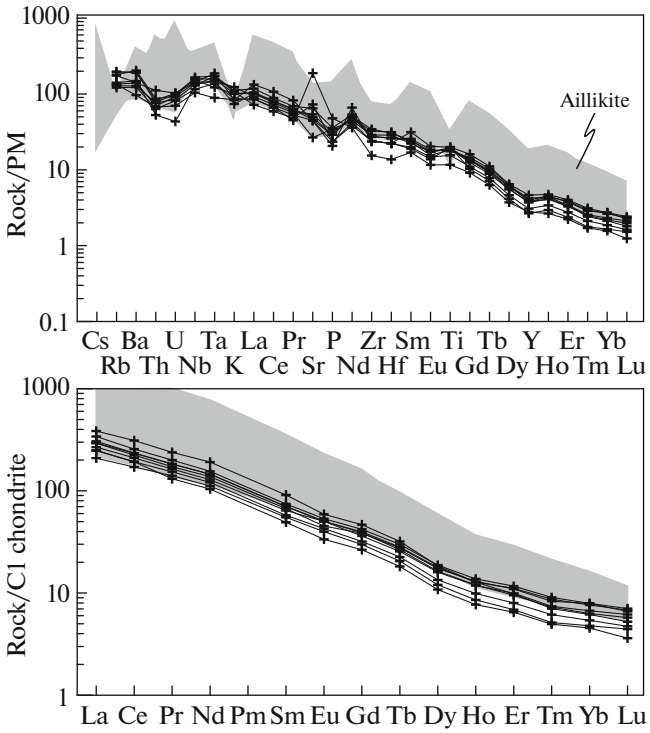

Fig. 11. Distribution spectra of rare and rare-earth elements normalized to primitive mantle and C1 chondrite according to (McDonough and Sun, 1995) in rocks of Ilbokichskaya-3 borehole (black crosses). Aillikite field according to (Tappe et al., 2006; Tappe et al., 2008).

Magmatism in Southwestern Siberia in the Early–Middle Devonian

The formation of commercial diamondiferous kimberlites in the SP is related to Devonian magmatism. Kimberlite formation in the central part of the SP was preceded by active manifestations of subalkali basaltic magmatism most characteristic of the Vilyui Rift in the eastern SP. The Vilyui Rift is the largest

Table 9. Results of Rb–Sr isotope studies of phlogopite and carbonate fractions and Ilb3-28 bulk samples

Sample	Description	Rb, μg/g	Sr, μg/g	$^{87}Rb/^{86}Sr$	$^{87}Sr/^{86}Sr$
Ilb3-28	Bulk sample	89.4	1634	0.1583 ± 8	0.704097 ± 15
Ilb3-28	Phlogopite	347	290	3.466 ± 9	0.722542 ± 15
Ilb3-28a*	Phlogopite	343	200	4.97 ± 1	0.731040 ± 15
Ilb3-28b*	Phlogopite	316	232	3.94 ± 1	0.725222 ± 15
Ilb3-28c*	Phlogopite	319	236	3.89 ± 1	0.724910 ± 15
Ilb3-28	Carbonate	2.2	3340	0.0019 ± 4	0.703292 ± 15

* Phlogopite samples after treatment with 10% acetic acid.

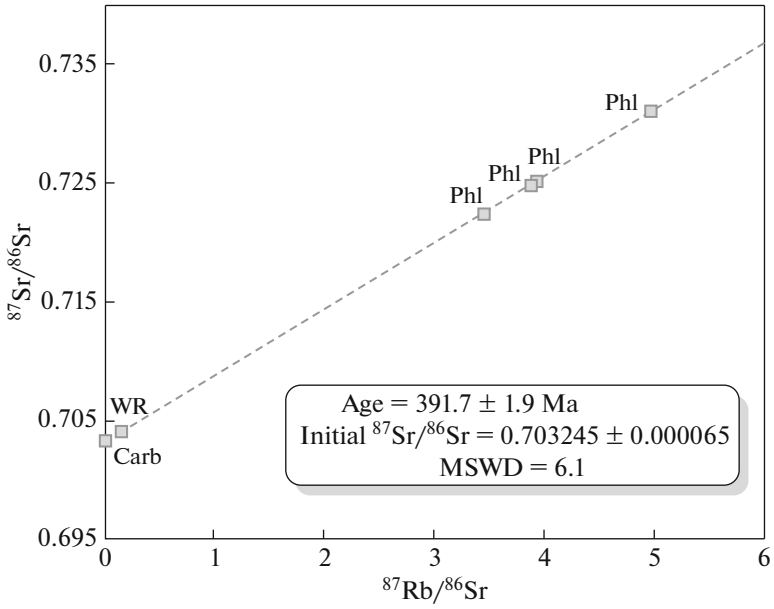

Fig. 12. Isochronic diagram for phlogopite (Phl), carbonate (Carb) and bulk aillikite sample (WR) of Ilb3-28.

Paleozoic structure of the SP, which represents a system of depressions composed of Middle–Upper Devonian volcanic, volcanosedimentary, and sedimentary (carbonate and terrigenous) strata with a total thickness of up to 6 km (Kiselev et al., 2006).

In the western SP, Devonian magmatism manifested itself in its southwestern folded framing and also within the Biryusa Terrane of the Siberian Craton as great bimodal effusions in many depressions, troughs, and grabens (Minusinsk, Tuva, etc., Agul in the near-Sayan Region) (Berzin, 1995; Vorontsov et al., 2010; Metelkin et al., 2012; Parfenov et al., 2003). The age of volcanic rocks is estimated as Early Devonian (Vorontsov et al., 2010): U–Pb dating by zircon is 407 ± 0.2 Ma (Kruk et al., 2002), and $^{40}Ar/^{39}Ar$ dating by bulk samples is 386 ± 4–402 ± 4 Ma, obtained for trachyrhyodacite and basalt of the Minusinsk Depression (Fedoseev, 2008). The magmatism involves (Vorontsov et al., 2010) normal, subalkali, and alkali rocks observed as both effusive facies (basalt, trachybasalt, nephelinite, phonotephrite, trachyte, trachydacite, etc.) and intrusive bodies (dolerite, teschenite, alkali syenite, etc.). The geochemical composition of the volcanic rocks is characterized by an increased contribution of the OIB-type enriched mantle source in troughs that considerably protruded deep into the paleocontinent; in contrast, in the outer parts of troughs, the rock geochemistry is substantially affected by the subduction components (Vorontsov et al., 2010).

The occurrence of potassium mafic lamprophyre (lamproitoid) containing microdiamonds was identified in the near-Sayan Region. The rocks are composed of clinopyroxene, olivine, and phlogopite phenocrysts and groundmass comprising salite, pseudomorphs after olivine, sanidine, phlogopite, Fe–Ti oxides and devitrified glass. The age of lamproitoids is estimated as Middle Paleozoic (Pokhilenko et al., 2012).

The geodynamic setting of Early Devonian magmatism is still a matter of debate. Most researchers suggest it is riftogenic in nature, but the causes of the riftogenesis are interpreted in different ways. According to (Berzin, 1995; Parfenov et al., 2003), Early Devonian riftogenesis was related to large strike-slips along the Kuznetsk–Altai shear and along the Major Fault of the Eastern Sayan Region. The Middle–Late Devonian was accompanied by changes in the geodynamic setting, and the southern margin of the SP replaced the passive margin conditions with an active margin, thus affecting the magmatism, which became calc–alkali, and restarting the subduction of the oceanic plate beneath the Siberian continent (Berzin, 1995). This viewpoint is consistent with paleoreconstructions for the Devonian period (400 Ma) given in (Metelkin et al., 2012). An alternative hypothesis is plume-related (Vorontsov et al., 2010). In the opinion of Vorontsov et al., Devonian magmatism was produced under the action of the mantle plume in the subduction zone. That is why its geochemical and isotopic–geochemical (Sr, Nd) features reflect the contribution of subduction material, including sediments, on the one hand, and mantle sources, such as N-MORB, on the other hand.

Hence, Early–Middle Devonian alkali–ultramafic magmatism could have formed in the southwestern craton part of the SP, most likely in remote back-arc conditions.

Forecasting Importance of Promising Primary Diamond Deposits in Southwest Siberia

The obtained estimate of the isotopic age of aillikite, defining it as a manifestation of Early Paleozoic (Early–Middle Devonian) alkali–ultramafic magmatism, is essential in studying Paleozoic magmatism in the southwest SP, in particular, in substantiating the diamond potential at this part of the craton. Today, a few metallogenic zoning approaches are used in the southwest SP.

According to (Dobretsov and Pokhilenko 2010; Dodin et al., 2008), the southwest SP contains the Tunguska diamondiferous subprovince (Fig. 13), which is promising for the detection of primary diamond deposits. The Ilbokich occurrence is located within the Baikit area (Fig. 13), which is promising for the detection of kimberlites (Dodin et al., 2008, Egorov, 2011). In the southwestern framing of the Tunguska Syneclise is the promising South Tunguska area, according to (Dobretsov and Pokhilenko 2010; Dodin et al., 2008), or the near-Sayan region, according to (Egorov, 2011).

Within the near-Sayan region (Egorov, 2011), there are Mesoproterozoic lamproites (Ingashi River occurrence) and Neoproterozoic kimberlites (Yarma River occurrence), as well as alkali–mafic rocks and carbonatites of the Zima Complex (Egorov, 2011; Dobretsov and Pokhilenko, 2010). Middle Paleozoic low-diamond lamproitoid occurrences of the near-Sayan Trough were identified in the same area (Pokhilenko et al., 2012). The existence of two (Middle Riphean and Middle Paleozoic) epochs of the formation of diamond-bearing kimberlite and/or lamproite bodies within the southern margin of the SP is confirmed by "ancient" Precambrian and Phanerozoic diamonds in placers of the Biryusa and Ingashet rivers (Egorov, 2011). This subprovince is considered highly promising for primary commercial diamonds (Dobretsov and Pokhilenko, 2010).

The Baikit Region (Egorov, 2011), in addition to the Ilbokich occurrence, includes two fields of Mesozoic alkali–ultramafic rocks the such as Chadobets and Taygikun–Nemba (Fig. 13). In addition, on the eastern slope of the Baikit Anteclise within the Uda–Tunguska mineragenic area (Fig. 13), there are a few promising sites (Egorov, 2011). Based on investigation data on the assemblages of accessory minerals and diamonds in the Late Devonian, Carboniferous, Permian, Jurassic, and Neogene–Quaternary intermediate reservoirs, it is assumed that the predicted kimberlite fields of this subprovince should be dated at the pre-Mesozoic. Garnets in Carboniferous conglomerates in the northern part of Baikit contain many low-Ca, high-Cr pyropes, which are characteristic of high-diamondiferous kimberlites and are completely absent in Mesozoic kimberlites in this subprovince (Dobretsov and Pokhilenko, 2010).

The discovery of the Ilbokich ultramafic lamprophyre occurrence—Middle Devonian aillikite—points to the existence of Early Paleozoic alkali–ultramafic magmatism in the northern part of the southwest SP and is consistent with forecasting reconstructions (Dobretsov and Pokhilenko 2010; Dodin et al., 2008), which has made it possible to identify the promising Baikit region within the Uda–Tunguska diamond-bearing mineragenic area (Egorov, 2011).

The age of Ilbokich aillikite, estimated at 391.7 ± 1.9 Ma, corresponds to the turn of the Early and Middle Devonian; this date is the closest to the boundary of 383.6 ± 3.0 Ma corresponding to the formation of commercial diamond-bearing kimberlites in the central part of the SP, in particular, Nakyn pipes (Kiselev et al., 2014); it is somewhat more ancient than the formation age of the commercial diamond-bearing pipes in the Daldyn–Alakit area and Minor Botuoba field (Agashev et al., 2004 and references therein). In the northern SP are sporadic occurrences of alkali–ultrabasic and carbonatite magmatism with ages corresponding to the turn of the Lower and Middle Devonian (about 397–393 Ma), such as carbonatites of the Tomtor Massif in the northern SP, with an age of 414–387 Ma (Vladykin et al., 2014), and one of pipes of the Anabar diamond district, with an age of 389 ± 12 Ma (Rb–Sr method, phlogopite; Zaitsev and Smelov, 2010). These data, together with the new data on the southern SP, give grounds to assume a large-scale phase of highly carbonate mantle metasomatism in the Early Devonian preceding the main period of kimberlite formation in the SP.

The formation of commercial diamondiferous kimberlites at the Nakyn and Minor Botuoba fields and, probably, Daldyn–Alakit kimberlites can be related to a Middle Paleozoic tectonothermal event in the east of the Siberian Craton, which is the best-defined in the Vilyui Rift as systems of rift troughs with sedimentary and volcanogenic filling ($D_{2\text{-}3}$–C_1) and extended mafic dike belts on the shoulders of rifts (Kiselev et al., 2006, 2014). Meanwhile, kimberlites formed within a longer time period of Middle Paleozoic basaltic magmatism in the shoulder area of the Vilyui Rift (Kiselev et al., 2014).

Despite the fact that the Ilbokich aillikite occurrence is located a considerable distance from Nakyn and Minor Botuoba kimberlites, it is situated in the southwestern end of the zone with NE-trending faults (Fig. 13), which can trace continuation of the northwest branch of the Vilyui Rift structure (?), as well as the Daldyn–Olenek mineragenic zone, which includes commercial diamondiferous kimberlite fields of the central part of the SP. This zone, being subparallel, is located north of the Angara–Vilyui mineragenic zone identified by (Egorov, 2011).

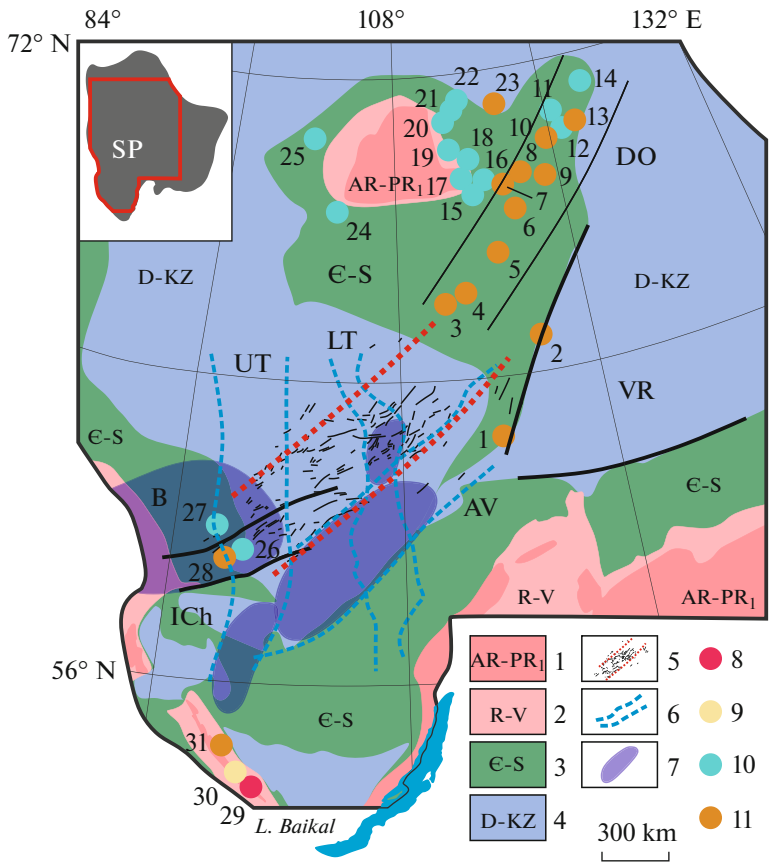

Fig. 13. Location of kimberlites and related rocks and identification of commercially promising areas. (1–4) Rock outcrops: (1) crystalline foundation of AR–PR_1 age, (2) R–V age, (3) Є–S age, (4) D–KZ age; (5) kimberlite magmatism-promising zone traced by NE-trending fault system; (6) mineragenic zones, according to (Egorov, 2011): (UT) Uda–Tunguska diamond-bearing mineragenic zone, (LT) Lena–Tunguska, (AV) Angara–Vilyui; (7) a contour of promising Baikit (B) diamond-bearing zone is shown with a light grey field, according to (Dobretsov and Pokhilenko, 2010; Dodin et al., 2008); (8–11) age of kimberlites and related rocks: (8) Mesoproterozoic, (9) Neoproterozoic, (10) Paleozoic, (11) Mesozoic. (DO) Daldyn–Olenek mineragenic zone. Numbers of kimberlite fields and occurrences of related rocks are shown in Fig. 1.

Forcasting Importance of Diamond Potential in Southwest Siberia

Such questions as the genetic relationship of ultramafic lamprophyre, kimberlite, and carbonatite, as well as their implications for forecasting commercially important kimberlite occurrences, remain debatable (Tappe et al., 2006, 2011; Lapin, 2001; etc.).

The occurrence of diamonds in ultramafic lamprophyre—aillikite—indicates, e.g., (Digonnet et al., 2000), the possible generation of their melts at large depths (over 150 km). Transitional varieties between aillikites and carbonatites, aillikites and orangeites (Tappe et al., 2008) suggest a genetic relationship of ultramafic lamprophyre with kimberlites within one large magmatic province or district, e.g., Mesozoic kimberlites and related rocks, including orangeite and ultramafic lamprophyre, transitional to carbonatite, in the northern Anabar District of the Yakut diamondiferous province (Bogatikov et al., 2004 Kharkiv and al., 1998), carbonatite and alkali picrate–alnoite in the Chadobets Elevation in the southwest SP (Lapin, 2001; Lapin and Lisitsyn, 2004; Lapin and Pyatenko, 1992), and aillikite and carbonatite in the Greenland–Labrador diamondiferous province within the North Atlantic Craton (Tappe et al., 2006, 2011).

It should be noted that large areas dominated by or enriched in ultramafic lamprophyre and/or alkali picrite spatially combined with kimberlite and carbonatite, as a rule, are not commercially diamondiferous. For example, Lapin (2001), based on a study of Chadobets rocks, suggests that rare-metal carbonatite complexes, which also contain alkali–ultrabasic differences, cannot be directly related to diamondiferous kimberlites.

Conversely, large diamondiferous areas where the role of carbonatite and alkali–ultramafic lamprophyre magmatism is minimum include commercial diamondiferous kimberlites, which are important primary diamond deposits in Russia, e.g., the Arkhangelsk diamond province (Bogatikov et al., 1999), where alkali

picrite and rocks, similar in composition to ultramafic lamprophyre, are characterized by a clear structural position in the area and are not combined with commercial diamondiferous kimberlites (Sablukov and Sablukova, 2008).

The finding of Devonian alkali–ultramafic lamprophyre in the Ilbokich occurrence is of dual predictive value. On the one hand, it points to the low probability of identifying large diamond-bearing deposits in close association with aillikite. On the other hand, it can indicate the possible occurrence of a large Devonian diamond province in this region, where diamondiferous kimberlites are structurally separated from aillikite. The relatively thick lithospheric mantle under the Tunguska Subprovince is favorable for the detection of diamond-bearing bedrock, because the conducting asthenosphere boundary under the studied area can exceed 180 km (Fig. 13) (Dashkevich, 1999).

CONCLUSIONS

Detailed petrographical, mineralogical, geochemical, and geochronological studies of Ilbokich ultramafic lamprophyres made it possible to establish the following:

(1) specific features in the mineral and chemical composition of the studied ultramafic lamprophyre point to its similarity to aillikite and, occasionally, to damtjernite;

(2) according to the Rb–Sr investigation data, ultramafic lamprophyre dikes intruded at the turn of the Early and Middle Devonian, about 392 Ma ago;

(3) review of the reconstructed geodynamic conditions in the southern SP in the Early–Middle Devonian period makes it possible to suggest that Early–Middle Devonian alkali–ultramafic magmatism occurrences in the southwestern craton part of the SP could have formed in rift zones, probably, in a remote back-arc setting;

(4) the identification of alkali–ultramafic lamprophyres in the Ilbokich wedge points to the existence of Early Paleozoic alkali–ultramafic magmatism in the northern part of the southwestern SP and is consistent with the forecasting reconstructions by Dobretsov and Pokhilenko (2010) and Dodin et al. (2008), who identified the promising Baikit region within the Uda–Tunguska diamond mineragenic area (Egorov, 2011);

(5) the finding of Devonian alkali–ultramafic lamprophyre is of dual predictive value: on the one hand, it is indicative of the low probability of identifying large diamond-bearing deposits in close association with aillikite, and on the other, it is indicative of the possible occurrence of a large Devonian diamond province in this area, where diamondiferous kimberlites are structurally separated from aillikites.

ACKNOWLEDGMENTS

We are grateful to Gazprom Geologorazvedka LLC for the materials. We thank A.I. Yakushev (Institute of Geology of Ore Deposits, Petrography, Mineralogy and Geochemistry, Russian Academy of Sciences) and V.K. Karandashev (Institute of Microelectronics Technology and High Purity Materials, Russian Academy of Sciences) for their assistance in analytical work. Microprobe investigations were carried out thanks to E.V. Kovalchuk (Institute of Geology of Ore Deposits, Petrography, Mineralogy and Geochemistry, Russian Academy of Sciences) and E.V. Guseva (Moscow State University). The study was partially carried out at the Laboratory for Local Research of Matter, Faculty of Geology, Department of Petrology, Moscow State University, using a JEOL JXA-8230 electronic probe microanalyzer acquired under the Program for Development of Moscow State University.

We thank V.V. Yarmolyuk (Institute of Geology of Ore Deposits, Petrography, Mineralogy and Geochemistry, Russian Academy of Sciences) for his valuable advice and constructive criticism. The work was supported by the Russian President Grant for State Support of Young Russian Scientists (grant no. MK-3410.2015.5) and by the Russian Foundation for Basic Research (project no. 16-05-00298).

REFERENCES

Agashev, A.M., Pokhilenko, N.P., Tolstov, A.V., et al., New age data on kimberlites from the Yakutian diamondiferous province, *Dokl. Earth Sci.,* 2004, vol. 399, no. 8, pp. 1142–1145.

Berzin, N.A., Tectonics of South Siberia and horizontal movements of continental crust, *Extended Abstract of Doctoral (Geol.-Min.) Dissertation*, Novosibirsk, 1995.

Bogatikov, O.A., Garanin, V.K., Kononova, V.A., et al., *Arkhangel'skaya almazonosnaya provintsiya (geologiya, petrografiya, geokhimiya i mineralogiya)* (Arkhangelsk Diamond Province: Geology, Petrography,m Geochemistry, and Mineralogy), Bogatikov, O.A., Eds., Moscow: MGU, 1999.

Bogatikov, O.A., Kononova, V.A., Golubeva, Yu.Yu., et al., Variations in chemical and isotopic compositions of the Yakutian kimberlites and their causes, *Geochem. Int.,* 2004, vol. 42, no. 9, pp. 799–821.

Bush, V.A., Structure of the Irinkeev-Chadobetsk aulacogene: evidence from complex aerogeophysical survey, *Sovrem. Aerogeofiz. Metody Tekhnol.,* 2009, vol. 1, no. 1, pp. 143–153.

Cohen, K.M., Finney, S.C., Gibbard, P.L., et al., The ICS international chronostratigraphic chart, *Episodes,* 2013, vol. 36, pp. 199–204.

Dashkevich, N.N., *Regional prediction of kimberlite magmatism in the southwestern Siberian Platform, Geologiya i poleznye iskopaemye Krasnoyarskogo kraya,* (Geology and Mineral Resources of Krasnoyarsk District), 1999, pp. 31–42.

Digonnet, S., Goulet, N., Bourne, J., et al., Petrology of the abloviak aillikite dykes, New Quebec: evidence for a Cambrian diamondiferous alkaline province in northeast-

ern North America, *Can. J. Earth Sci.,* 2000, vol. 37, pp. 517–533.

Dobretsov, N.L. and Pokhilenko, N.P., Mineral Resources and development in the Russian Arctic, *Russ. Geol. Geophys.,* 2010, vol. 51, no. 1, pp. 126–141.

Dodin, D.A., Ivanov, V.L., and Kaminskii, V.D., Russian Arcctic—large raw mineral base of Russia (on 60th anniversary of VNII Okeangeologiya), *Litosfera,* 2008, vol. 4, pp. 76–92.

Egorov, K.N. and Mikhail, M., Odintsov's contribution to development of the mineral and raw materials complex of the Sastern Siberia, *Geodyn. Tectonophys,* 2011, vol. 2, no. 4, pp. 325–340.

Fedoseev, G.S., The role of magmatism in age specification of Devonian continental trough deposits: evidence from the Minusa Basin, Western Siberia, Russia, *Bull. Geosci.,* 2008, vol. 83, no. 4, pp. 473–480.

Kargin, A.V., Golubeva, Yu.Yu., and Kononova, V.A., Kimberlites of the Daldyn–Alakit region (Yakutia): spatial distribution of the rocks with different chemical characteristics, *Petrology,* 2011, vol. 19, no. 5, pp. 496–520.

Khar'kiv, A.D., Zinchuk, N.N., and Kryuchkov, A.I., *Korennye mestorozhdeniya almazov Mira (Primary Diamond Deposits of the Worlds)*, Moscow: Nedra, 1998.

Kirichenko, V.T., Zuev, V.K., Perfilova, O.Yu., et al., *Gosudarstvennaya geologicheskaya karta Rossiiskoi Federatsii. Masshtab 1: 1000000 (tret'e pokolenie). Seriya Angaro-Eniseiskaya. List O-47—Bratsk. Ob"yasnitel'naya zapiska* (State Geological Map of the Russian Federation on a Scale 1: 1000000 (Third Generation). Angara–Yenisei Series. Sheet O-47—Bratsk. Explanatory Notes), Glukhov, Yu.S., Ed., St. Petersburg: Kartograficheskaya fabrika VSEGEI, 2012.

Kiselev, A.I., Yarmolyuk, V.V., Egorov, K.N., et al., Middle Paleozoic basic magmatism of the northwestern Vilyui Rift: composition, sources, and geodynamics, *Petrology,* 2006, vol. 14, no. 6, pp. 588–608.

Kiselev, A.I., Yarmolyuk, V.V., Ivanov, A.V., and Egorov, K.N., Middle Paleozoic basaltic and kimberlitic magmatism in the northwestern shoulder of the Vilyui Rift, Siberia: relations in space and time, *Russ. Geol. Geophys.,* 2014, vol. 55, no. 2, pp. 144–152.

Kontorovich, A.E., Belyaev, S.Yu., and Kontorovich, A.A., Tectonic map of the Vendian–Lower Paleozoic structural stage of teh Lena–Tunguska petroleum province, Siberian Platform, *Russ. Geol. Geophys.,* 2009, vol. 50, no. 8, pp. 649–659.

Kruk, N.N., Babin, G.A., Vladimirov, A.G., et al., Devonian-like magmatism of East Sayan (U-Pb isotopic researches), in *Petrology of Magmatic and Metamorphic Complexes 3,* Chernyshov, A.I., Ed., Tomsk, 2002, pp. 189–193.

Lapin, A.V. and Pyatenko, I.K., Chadobetsk complex of ultrabasic–alkaline rocks and carbonatites: new data on composition, structure, and conditions of formation, *Izv. Akad. Nauk SSSR, Ser. Geol.,* 1992, no. 6, pp. 88–101.

Lapin, A.V., Kimberlites of the Chadobets Uplift in relation with problem of formation–metallogenic analysis of platform alkaline ultrabasic magmatic rocks, *Otechestvennaya Geol.,* 2001, no. 4, pp. 30–35.

Lapin, A.V. and Lisitsin, D.V., Mineral typomorphism of the alkalne ultrabasic rocks of the Chadobets Uplift, *Otechestvennaya Geol.,* 2004, no. 6, pp. 83–93.

McDonough, W.F. and Sun, S., S. The composition of the Earth, *Chem. Geol.*, 1995, vol. 120, nos. 3–4, pp. 223–253.

Metelkin, D.V., Vernikovskii, V.A., and Kazanskii, A.Yu., Tectonic evolution of the Siberian paleocontinent from the Neoproterozoic to the Late Mesozoic: paleomagnetic record and reconstructions, *Russ. Geol. Geophys.,* 2012, vol. 53, no. 7, pp. 675–688.

Mitchell, R.H., *Kimberlites, Orangeites, and Related Rocks,* Springer, 1995.

Parfenov, L.M., Berzin, N.A., and Khanchuk, A.I., Model of formation of the Pacific and Northeastern Asian orogenic belts, *Tikhookean. Geol.,* 2003, vol. 22, no. 6, pp. 7–41.

Patino Douce, A.E., Roden, M.F., Chaumba, J., et al., Compositional variability of terrestrial mantle apatites, thermodynamic modeling of apatite volatile contents, and the halogen and water budgets of planetary mantles, *Chem. Geol.,* 2011, vol. 288.

Petrograficheskii kodeks Rossii. Magmaticheskie, metamorficheskie, metasomaticheskie, impaktnye obrazovaniya (Petrographic Code of Russia: Magmatic, Metamorphic, Metasomatic, and Impact Rocks), Bogatikov O.A., Petrov O.V., Morozov A.F., Eds., St. Petersburg, 2009.

Pokhilenko, N.P., Afanas'ev, V.P., Sobolev, N.V., et al., Stages of kimberlite magmatism of the Siberian Platform and their productivity: tendencies in the formation and prediction of primary diamond deposits of different genetic types, new prospective regions, *Problemy mineragenii Rossii,* (Metallogenic Problems of Russia), Rundkvist D.V., Bortnikov N.S., Safonov Yu.G., Eds., Moscow: GTs RAN, 2012, pp. 265–285.

Prelevic, D., Foley, S.F., Romer, R.L., et al., Tertiary ultrapotassic volcanism in Serbia: constraints on petrogenesis and mantle source characteristics, *J. Petrol.,* 2005, vol. 46, no. 7, pp. 1443–1487.

Sablukov, S.M. and Sablukova, L.I., Asthenospheric effect on the mantle substrate and diversity of kimberlite rocks in Zimni Bereg (Arkhangelsk Province), *9th International Kimberlite Conference,* Frankfurt, 2008, P. 9IKC–A–00162

Sazonova, L.V., Nosova, A.A., Kargin, A.V., et al., Olivine from the Pionerskaya and V. Grib kimberlite pipes, Arkhangelsk diamond province, Russia: types, composition, and origin, *Petrology,* 2015, vol. 23, no. 3, pp. 227–258.

Smelov, A.P. and Timofeev, V.F., The age of the north Asian cratonic basement: an overview, *Gondwana Res.,* 2007, vol. 12, no. 3, pp. 279–288.

Starosel'tsev, V.S., Identifying paleorifts as promising tectonic elements for active oil and gas generation, *Russ. Geol. Geophys.,* 2009, vol. 50, no. 4, pp. 350–356.

Steiger, R.H. and Jager, E., Subcommission on geochronology: convention on the use of decay constants in geo- and cosmochronology, *Earth Planet. Sci. Lett.,* 1977, vol. 36, no. 3, pp. 359–362.

Tacker, R.C. and Stormer, J.C., A thermodynamic model for apatite solid solutions, applicable to high-temperature geologic problems, *Am. Mineral.,* 1989, vol. 74, nos 7-8, pp. 877–888.

Tappe, S., Foley, S.F., Jenner, G.A., et al., Integrating ultramafic lamprophyres into the IUGS classification of igneous rocks: rationale and implications, *J. Petrol.,* 2005, vol. 46, no. 9, pp. 1893–1900.

Tappe, S., Foley, S.F., Jenner, G.A., et al., Genesis of ultramafic lamprophyres and carbonatites at Aillik Bay, Labrador: a consequence of incipient lithospheric thinning beneath the North Atlantic Craton, *J. Petrol.,* 2006, vol. 47, no. 7, pp. 1261–1315.

Tappe, S., Foley, S.F., Kjarsgaard, B.A., et al., Between carbonatite and lamproite - diamondiferous Torngat ultramafic lamprophyres formed by carbonate-fluxed melting of cratonic Marid-type metasomes, *Geochim. Cosmochim. Acta,* 2008, vol. 72, pp. 3258–3286.

Tappe, S., Pearson, D.G., Nowell, G., et al., A fresh isotopic look at Greenland kimberlites?: cratonic mantle lithosphere imprint on deep source signal, *Earth Planet. Sci. Lett.,* 2011, vol. 305, nos 1-2, pp. 235–248.

Vladykin, N.V., Kotov, A.B., Borisenko, A.S., et al., Age boundaries of formation of the Tomtor alkaline–ultramafic pluton: U–Pb and $^{40}Ar/^{39}Ar$ geochronological studies, *Dokl. Earth Sci.,* 2014, vol. 454, no. 1, pp. 7–11.

Vorontsov, A.A., Yarmolyuk, V.V., and Fedoseev, G.S., Isotopic and geochemical zoning of Devonian magmatism in the Altai–Sayan rift system: composition and geodynamic nature of mantle sources, *Petrology,* 2010, vol. 18, no. 6, pp. 596–609.

Zaitsev, A.I. and Smelov, A.P., *Izotopnaya geokhronologiya porod kimberlitovoi formatsii Yakutskoi provintsii* (Isotopic Geochronology of the Kimberlite Rocks of the Yakutsk Province), Shkodzinskii, V.S Eds., Yakutsk: IGABM SO RAN, 2010.

Translated by E. Maslennikova